

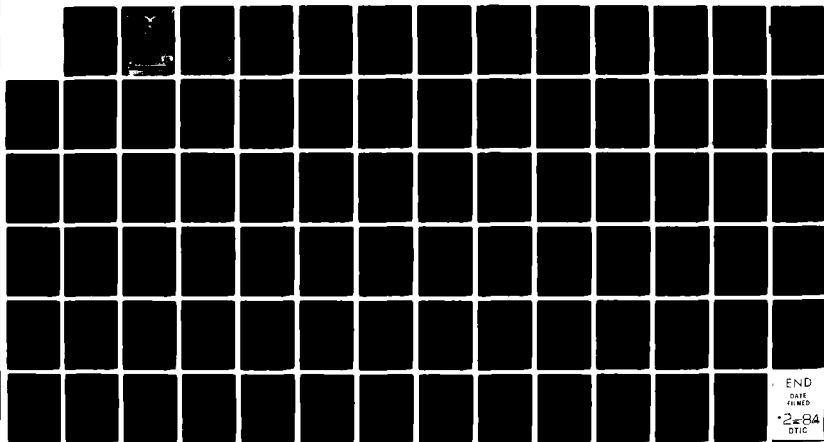
AD-A136 921

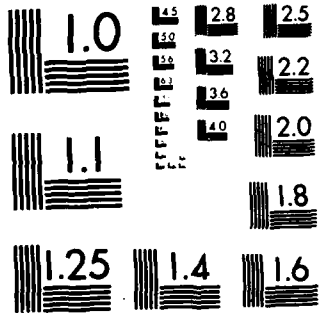
THE EFFECT OF TRAILING VORTICES ON THE PRODUCTION OF  
LIFT ON AN AIRFOIL U. (U) AIR FORCE INST OF TECH  
WRIGHT-PATTERSON AFB OH SCHOOL OF ENGI... K W TUPPER  
DEC 83 AFIT/GAE/AA/83D-24 F/G 20/4

1 / 1

UNCLASSIFIED

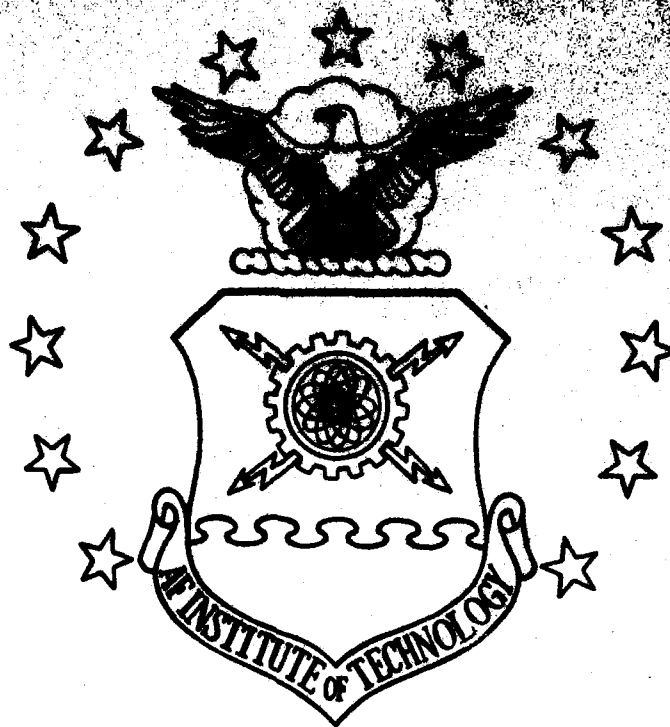
NL





MICROCOPY RESOLUTION TEST CHART  
NATIONAL BUREAU OF STANDARDS-1963-A

AD A136921



THE EFFECT OF TRAILING VORTICES ON THE  
 PRODUCTION OF LIFT ON AN AIRFOIL  
 UNDERGOING A CONSTANT RATE OF  
 CHANGE OF ANGLE OF ATTACK

THESIS

Kenneth W. Tupper  
 Captain, USAF

AFIT/GAE/AA/83D-24

THIS IS A COPY

DTIC  
 ELECTE  
 JAN 18 1984  
 S D E

DEPARTMENT OF THE AIR FORCE  
 AIR UNIVERSITY  
**AIR FORCE INSTITUTE OF TECHNOLOGY**

Wright-Patterson Air Force Base, Ohio

84 01 17 087

THIS COPY IS NOT TO BE REPRODUCED OR TRANSMITTED IN ANY FORM OR BY ANY MEANS, ELECTRONIC OR MECHANICAL, INCLUDING PHOTOCOPYING, RECORDING, OR BY ANY INFORMATION STORAGE AND RETRIEVAL SYSTEM.

AFIT/GAE/AA/83D-24

①

THE EFFECT OF TRAILING VORTICES ON THE  
PRODUCTION OF LIFT ON AN AIRFOIL  
UNDERGOING A CONSTANT RATE OF  
CHANGE OF ANGLE OF ATTACK

THESIS

Kenneth W. Tupper  
Captain, USAF

AFIT/GAE/AA/83D-24

DTIC  
ELECTE  
S JAN 13 1984 D  
E

Approved for public release; distribution unlimited

THE EFFECT OF TRAILING VORTICES ON THE PRODUCTION  
OF LIFT ON AN AIRFOIL UNDERGOING A CONSTANT  
RATE OF CHANGE OF ANGLE OF ATTACK

THESIS

Presented to the Faculty of the School of Engineering  
of the Air Force Institute of Technology  
Air University

In Partial Fulfillment of the  
Requirements for the Degree of  
Master of Science in Aeronautical Engineering



Kenneth W. Tupper, B.S.  
Captain, USAF

December 1983

|                      |                                     |
|----------------------|-------------------------------------|
| <b>Accession For</b> |                                     |
| NTIS GRA&I           | <input checked="" type="checkbox"/> |
| DTIC TAB             | <input type="checkbox"/>            |
| Unannounced          | <input type="checkbox"/>            |
| Justification        |                                     |
| By _____             |                                     |
| Distribution/        |                                     |
| Availability Codes   |                                     |
| Dist                 | Avail and/or<br>Special             |
| A-1                  |                                     |

Approved for public release; distribution unlimited

## Preface

The purpose of this study was to investigate the effect a trailing vortex wake has on an airfoil undergoing a constant rate of change of angle of attack,  $\dot{\alpha}$ , in two-dimensional, incompressible, irrotational flow. Potential flow theory, conformal mapping by the Joukowski transformation, and numerical integration and differentiation techniques were used to develop a computer algorithm to model the problem. Once the program was formulated, it was used to solve the impulsive-start problem of airfoil motion. The results were found to be in excellent agreement with the results obtained by others. When applied to the constant rate-of-change of angle-of-attack problem, the results showed that a trailing vortex wake has a measurable and predictable effect on the production of lift on an airfoil undergoing a constant  $\dot{\alpha}$ .

The results of this work, taken alone, are helpful in understanding the phenomena known as dynamic stall, but coupled with existing boundary-layer studies the results may lead to additional understanding of the phenomena. More specifically, the computer program developed here could be used to more realistically predict the inviscid flow about a pitching airfoil as it approaches the dynamic-stall conditions. †

This study could never have been completed without the help of others. I owe a great deal of thanks to Major Eric Jumper, who not only posed this problem to me, but who also

provided invaluable assistance throughout the investigation. I also wish to thank Lt. Colonel Michael Smith for his help with potential flow theory and his expert advise regarding the writing of this report. Finally, I wish to thank my wife Anneliese for her translations of the German references and, most importantly, for her help in keeping the work involved in this thesis in proper perspective.

Kenneth W. Tupper

Table of Contents

|  | Page |
|--|------|
| Preface . . . . .  | ii   |
| List of Figures . . . . .  | v    |
| List of Tables. . . . .  | vii  |
| Abstract. . . . .  | viii |
| I. Introduction. . . . .   | 1    |
| II. Solution Development. . . . .  | 3    |
| Solution Overview . . . . .  | 3    |
| Equations for Flow About a Cylinder . . . . .                            | 5    |
| Joukowski Transformation. . . . .  | 10   |
| Determination of Strength of Vortices . . . . .                          | 11   |
| Velocities Induced at Discrete Vortices<br>and on the Cylinder . . . . . | 14   |
| Circulation About the Airfoil . . . . .                                  | 17   |
| Velocity in the Airfoil Frame . . . . .                                  | 18   |
| Pressure, Lift, Vorticity Distribution<br>on the Airfoil. . . . .        | 19   |
| Numerical Solution Process. . . . .                                      | 21   |
| III. Results . . . . .   | 25   |
| Numerical Method Verification . . . . .                                  | 25   |
| Application to Constant- $\alpha$ Flow. . . . .                          | 41   |
| Selection of Standard Starting<br>Conditions. . . . .                    | 41   |
| General Effect of $\alpha$ on $C_{l\alpha}$ . . . . .                    | 47   |
| Effect of Airfoil Thickness on $\alpha$<br>Effect. . . . .               | 47   |
| Effect of Airfoil Camber on $\alpha$ Effect. . . . .                     | 50   |
| IV. Conclusion. . . . .  | 54   |
| V. Recommendation. . . . .   | 57   |
| Appendix: Computer Program . . . . .                                     | 58   |
| Bibliography. . . . .  | 66   |
| Vita. . . . .  | 68   |



List of Figures

| Figure   | Page |
|--|------|
| 1. Cylinder in Free Stream at Angle of Attack with Vortex and Image. . . . .   | 6    |
| 2. Planes of the Joukowski Transformation. . . . .   | 12   |
| 3. Build-up of Circulation on an Impulsively-Started Flat Plate. . . . .   | 26   |
| 4. Build-up of $C_l$ on an Impulsively-Started Flat Plate . . . . .  | 27   |
| 5. Coefficient of Lift vs. Distance Traveled (Effect of $\Delta t^*$ on Numerical Solution) . . . . .  | 29   |
| 6. Dimensionless Vorticity Distribution on a Flat Plate, $\alpha = 0.1$ radians. . . . .   | 30   |
| 7. Pressure Difference Distribution on a Flat Plate, $\alpha = 0.1$ radians. . . . .   | 31   |
| 8. Wake Vortex Sheet Roll-up for a Flat Plate, $\alpha = 0.1$ radians. . . . .   | 33   |
| 9. Build-up of $C_l$ on a 25.5% Thick Symmetric Joukowski Airfoil . . . . .  | 34   |
| 10. Wake Vortex Sheet Roll-up for a Flat Plate, $\alpha = 10^\circ$ (Predictor-Corrector vs. Present Method) . . . . .                         | 36   |
| 11. Dimensionless Vorticity Distribution, 25.5% Thick Symmetric Joukowski Airfoil, $\alpha = 0.1$ radians. . . . .                             | 39   |
| 12. Pressure Difference Distribution, 25.5% Thick Symmetric Joukowski Airfoil, $\alpha = 0.1$ radians . . . . .                                | 40   |
| 13. Coefficient of Lift vs. Angle of Attack (Effect of Start Time to Begin $\alpha$ for $\alpha_0 = 0^\circ$ ). . . . .                        | 42   |
| 14. Coefficient of Lift vs. Angle of Attack (Effect of Start Time to Begin $\alpha$ for $\alpha_0 = 5^\circ$ ). . . . .                        | 44   |
| 15. Coefficient of Lift vs. Angle of Attack (Effect of Initial Angle of Attack ( $C_l$ at 90% Steady-State Value) to Begin $\alpha$ ). . . . . | 45   |

| Figure   | Page |
|--|------|
| 16. Coefficient of Lift vs. Angle of Attack (Effect of $\Delta t^*$ on Curve Slope). . . . .                               | 46   |
| 17. Coefficient of Lift vs. Angle of Attack (Effects of $\dot{\alpha}$ for 15% Thick Symmetric Joukowski Airfoil). . . . . | 48   |
| 18. Coefficient of Lift vs. Angle of Attack (Slope Change as Angle of Attack Increases at Constant $\alpha$ ). . . . .     | 49   |
| 19. Airfoil Thickness Effect on the Slope of the $C_{\ell}$ vs. $\alpha$ Curve for Constant $\dot{\alpha}$ . . . . .       | 51   |
| 20. Airfoil Camber Effect on the Slope of the $C_{\ell}$ vs. $\alpha$ Curve for Constant $\dot{\alpha}$ . . . . .          | 53   |
| 21. Flat Plate $C_{\ell\alpha}$ Changes as a Function of $\dot{\alpha}^*$ . . . . .  | 55   |

List of Tables

| Table   | Page |
|---|------|
| I. Comparison of $C_l$ Calculated by Simple Predictor Method to $C_l$ Calculated by Predictor-Corrector Method. Flat Plate Airfoil, $\alpha = 10^\circ$ . . . . . | 38   |
| II. Comparison of $C_l$ Calculated by Simple Predictor Method to $C_l$ Calculated by Predictor-Corrector Method. Flat Plate Airfoil, $\alpha^* = 0.035$ . . . . . | 38   |

Abstract

This study explored the effect of a trailing vortex wake on the production of lift on an airfoil undergoing a constant rate of change of angle of attack,  $\dot{\alpha}$ . The study showed that when an airfoil encounters a constant- $\dot{\alpha}$  flow, the trailing vortex wake acts to suppress the slope of the airfoil's  $C_l$  vs.  $\alpha$  curve. The change in magnitude of this effect as a function of airfoil thickness and camber was also investigated.

Potential flow theory was used to model the flow about a two-dimensional circular cylinder, and that flow was transformed to flow about an airfoil by the Joukowski transformation. The trailing vortex wake was modeled by a sequence of discrete point vortices, and the pitching motion of the airfoil was modeled by a series of small incremental changes in angle of attack,  $\Delta\alpha$ , over a short period of time,  $\Delta t$ . The rate of change of angle of attack,  $\dot{\alpha}$ , was then defined as  $\Delta\alpha/\Delta t$ . After each time change  $\Delta t$ ,  $\alpha$  was changed by an amount  $\Delta\alpha$ . A discrete vortex was introduced into the wake at a distance  $U_\infty\Delta t$  behind the airfoil trailing edge, and a bound vortex of equal strength but opposite sense was introduced to satisfy the Kutta condition and keep the total circulation in the flow field equal to zero. As each new vortex pair was introduced, all other trailing vortices were

assumed to move in the wake by a distance  $U\Delta t$ , where  $U$  is the velocity induced at a vortex position by all other trailing vortices, the bound vortices, and the free stream flow. The unsteady Bernoulli equation was solved using numerical integration and differentiation techniques to determine pressure difference distribution, vorticity distribution, and coefficient of lift on the airfoil for that instant in time. This information was then used to investigate the overall effect of constant- $\dot{\alpha}$  flow as well as the effect of thickness and camber on the constant- $\dot{\alpha}$  problem, and simple rules for predicting the effects were developed.

THE EFFECT OF TRAILING VORTICES ON THE PRODUCTION  
OF LIFT ON AN AIRFOIL UNDERGOING A CONSTANT  
RATE OF CHANGE OF ANGLE OF ATTACK

I. Introduction

It has been determined experimentally that an airfoil pitching at some rate of change of angle of attack  $\dot{\alpha}$  stalls at a higher angle of attack  $\alpha$  than the static stall  $\alpha$ . Max von Kramer first showed this with his experiments in 1932 (1), where he held the airfoil fixed in space and rotated the flow over the airfoil to create an  $\dot{\alpha}$ . Deekens and Kuebler (2) and Daley (3) ran similar experiments for a constant  $\dot{\alpha}$ , but rather than rotating the flow, they rotated the airfoil in a constant velocity free stream to produce their  $\dot{\alpha}$ . In all three cases the stall occurred at a higher angle of attack than the static-stall angle of attack. However, because of the different methods used to produce  $\dot{\alpha}$ , Kramer's results showed a much smaller change in stall angle of attack than did Deekens and Kuebler and Daley.

Following these experiments, attempts have been made to analytically model the case of an airfoil undergoing a constant  $\dot{\alpha}$ . Docken (4) and Lawrence (5) have tackled the problem using a momentum integral method, but both assumed in their solution that the effect of the trailing vortices in

the airfoil wake was small and could be neglected. Thus, they assumed that the inviscid flow velocity outside the airfoil boundary layer at any angle of attack was that which would exist in the steady state at that angle of attack. It is the intent of this thesis to determine the validity of that assumption by analyzing the effect a trailing vortex wake has on the inviscid flow field about an airfoil undergoing a constant rate of change in angle of attack (i.e., constant  $\dot{\alpha}$ ). The effect of the trailing vortex wake on the flow about the airfoil can be analyzed by determining how the vorticity distribution and pressure difference distribution on the airfoil develop under the influence of the  $\dot{\alpha}$  (taking the trailing wake into account), and by observing the effect of the  $\dot{\alpha}$  on the  $C_l$  vs.  $\alpha$  curve.

## II. Solution Development

### Solution Overview

Consider an airfoil at an angle of attack which undergoes an impulsively started motion of velocity  $U_\infty$ . Assume the airfoil is immersed in an incompressible, inviscid fluid. Under these circumstances, a stagnation point of the flow would occur on the upper surface of the airfoil. This would imply an infinite velocity at the airfoil trailing edge. It is known, however, that the flow at the trailing edge of such an airfoil becomes smooth and has a finite velocity. This is known as the Kutta condition. Imposing the Kutta condition requires the formation of circulation around the airfoil to move the stagnation point to the trailing edge. This circulation can be modeled as a vortex bound to the airfoil. The total circulation in the flow must remain equal to zero by Kelvin's theorem, and thus circulation in the opposite sense is shed in the form of a discrete vortex into the airfoil wake. The strength of this vortex is just equal and opposite to that of the bound vortex on the airfoil. The equal and opposite strengths of the bound and shed vortices are just sufficient to satisfy the Kutta condition and Kelvin's theorem.

Thus, when the airfoil at angle of attack is impulsively started, circulation about the airfoil develops, and a wake vortex is shed. After a time  $\Delta t$ , this shed vortex is arbitrarily assumed to be at a distance  $U_\infty \Delta t$  from the trailing



edge (6:21). The bound vortex and shed vortex both affect the flow about the airfoil, and their strengths are such that the Kutta condition at the trailing edge is satisfied. Knowing the strengths of these vortices, the instantaneous values of circulation about the airfoil, as well as the pressure difference distribution, vorticity distribution, and coefficient of lift on the airfoil can be calculated. After another time  $\Delta t$ , the shed vortex has moved further downstream by a distance  $U_{sv}\Delta t$ , where  $U_{sv}$  is the velocity at the shed vortex location imposed by the free stream and all other vortices, including the bound vortex. In cases other than the impulsive-start problem, the angle of attack may also have changed by some amount equal to  $\dot{\alpha}\Delta t$ , where  $\dot{\alpha}$  is the average rate-change of angle of attack over the given time period  $\Delta t$ . The strength of the first shed vortex remains fixed, and thus another bound vortex and shed vortex must be introduced to keep the Kutta condition satisfied. This second shed vortex is assumed to be at a distance  $U_{\infty}\Delta t$  behind the trailing edge. The equal and opposite strengths of these new bound and shed vortices are again determined by imposing the Kutta condition. Now, for this new instant in time, the instantaneous values of airfoil circulation, pressure difference distribution, vorticity distribution, and coefficient of lift can once again be calculated. This process can be repeated for any number of discrete time steps  $\Delta t$  desired, and for that matter any  $\dot{\alpha}(t)$ , although in this study  $\dot{\alpha}$  was held constant. By

following this method, a time history of the development of circulation, pressure difference distribution, vorticity distribution, and coefficient of lift on the airfoil can be observed.

### Equations for Flow About a Cylinder

When solving a problem in two-dimensional incompressible, irrotational flow, it is often useful to make use of conformal mapping. In this case, the problem is solved for flow about a two-dimensional cylinder, then the Joukowski transformation is used to find the solution for a Joukowski airfoil.

Consider the flow of an incompressible, irrotational fluid in the  $o$ -plane. The flow is inclined at an angle  $\alpha$  to the  $x$ -axis (see Fig. 1). The stream function  $\psi$  and potential function  $\phi$  for this flow are given by (7:245):

$$\psi = U_{\infty}(Y \cos \alpha - X \sin \alpha) \quad (1)$$

$$\phi = U_{\infty}(X \cos \alpha + Y \sin \alpha) \quad (2)$$

where  $U_{\infty}$  is the magnitude of the free stream velocity.

If a doublet of strength  $K$ , axis inclined at angle  $\alpha$  to the  $X$ -axis, is placed at the origin of the  $o$ -plane, the stream function  $\psi$  and potential function  $\phi$  are given by:

$$\psi = \frac{-K}{2\pi} \left[ \frac{Y \cos \alpha - X \sin \alpha}{X^2 + Y^2} \right] \quad (3)$$

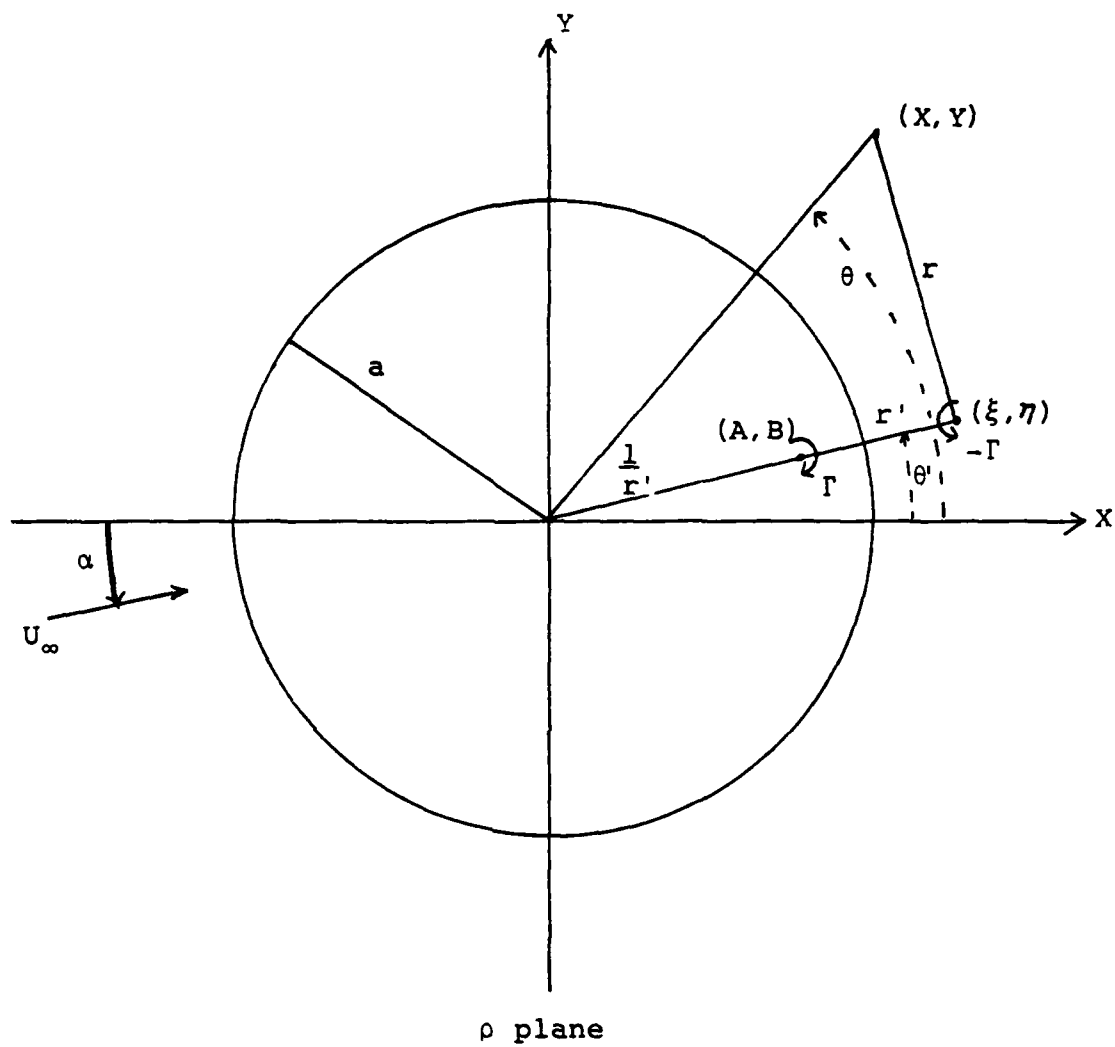


Fig. 1. Cylinder in Free Stream at Angle of Attack With Vortex and Image

$$\phi = \frac{K}{2\pi} \left[ \frac{X \cos \alpha + Y \sin \alpha}{X^2 + Y^2} \right] \quad (4)$$

Since stream functions and potential functions are linear, they may be superimposed to create new flows. Therefore, the stream and potential functions for a doublet in a uniform free stream at angle  $\alpha$  to the X-axis can be written as:

$$\begin{aligned} \psi &= U_{\infty}(Y \cos \alpha - X \sin \alpha) - \frac{K}{2\pi} \left[ \frac{Y \cos \alpha - X \sin \alpha}{X^2 + Y^2} \right] \\ &= (Y \cos \alpha - X \sin \alpha) \left[ U_{\infty} - \frac{K}{2\pi} \frac{1}{X^2 + Y^2} \right] \end{aligned} \quad (5)$$

$$\begin{aligned} \phi &= U_{\infty}(X \cos \alpha + Y \sin \alpha) + \frac{K}{2\pi} \left[ \frac{X \cos \alpha + Y \sin \alpha}{X^2 + Y^2} \right] \\ &= (X \cos \alpha + Y \sin \alpha) \left[ U_{\infty} + \frac{K}{2\pi} \frac{1}{X^2 + Y^2} \right] \end{aligned} \quad (6)$$

If strength  $K$  is such that  $K/2\pi U_{\infty} = a^2$ , where  $a$  is the radius of a cylinder, then the zero streamline will be the line along which  $Y \cos \alpha = X \sin \alpha$  and the cylinder of radius  $a$ , centered at the origin (8:89). The stream function and potential function are now:

$$\psi = U_{\infty}(Y \cos \alpha - X \sin \alpha) \left[ 1 - \frac{a^2}{X^2 + Y^2} \right] \quad (7)$$

$$\phi = U_{\infty}(X \cos \alpha + Y \sin \alpha) \left[ 1 + \frac{a^2}{X^2 + Y^2} \right] \quad (8)$$

Next, consider a vortex of strength  $-\Gamma$  located at  $(\xi, \eta)$  in the  $o$ -plane. If a vortex of strength  $\Gamma$  is placed at point  $(A, B)$  such that  $(A, B)$  is the inverse point of  $(\xi, \eta)$  about the surface of the cylinder of radius  $a$ , (i.e.,  $|\xi, \eta| = 1/|A, B|$ ), then the surface of the cylinder remains a streamline by the circle theorem (9:84, 85), and the total circulation remains zero. The stream and potential functions for a line vortex are given by (8:82)

$$\psi = \frac{\Gamma}{2\pi} \ln(r) \quad (9)$$

$$\vartheta = \frac{-\Gamma}{2\pi} \theta \quad (10)$$

where  $r$  is the distance from the vortex to the point in the  $o$ -plane where  $\psi$  and  $\vartheta$  are evaluated, and  $\theta$  is the angle measured counterclockwise from the  $x$ -axis to  $r$ . Adding  $\psi$  and  $\vartheta$  for each vortex in the pair yields

$$\psi = \frac{\Gamma}{2\pi} \ln \left[ ((X-A)^2 + (Y-B)^2)^{\frac{1}{2}} \right] - \frac{\Gamma}{2\pi} \ln \left[ ((X-\xi)^2 + (Y-\eta)^2)^{\frac{1}{2}} \right] \quad (11)$$

$$\vartheta = \frac{\Gamma}{2\pi} \arctan \left[ \frac{X-\xi}{Y-\eta} \right] - \frac{\Gamma}{2\pi} \arctan \left[ \frac{X-A}{Y-B} \right] \quad (12)$$

Note that  $A = (1/r') \cos \theta'$ ,  $B = (1/r') \sin \theta'$ , and since  $\cos \theta' = \xi/r'$ ,  $\sin \theta' = \eta/r'$  (see Fig. 1), then

$$A = \frac{\xi}{\xi^2 + \eta^2} \quad (13)$$

$$B = \frac{\eta}{\xi^2 + \eta^2} \quad (14)$$

After using the trigonometric identity (8:86)

$$\arctan \alpha - \arctan \beta = \arctan \left[ \frac{\alpha - \beta}{1 + \alpha\beta} \right] \quad (15)$$

and performing some algebraic manipulation, one derives

$$\psi = \frac{\Gamma}{4\pi} \ln \left[ \frac{(X-A)^2 + (Y-B)^2}{(X-\xi)^2 + (Y-\eta)^2} \right] \quad (16)$$

$$\phi = \frac{\Gamma}{2\pi} \arctan \left[ \frac{(X-\xi)(Y-B) - (X-A)(Y-\eta)}{(Y-\eta)(Y-B) + (X-\xi)(X-A)} \right] \quad (17)$$

Finally, let there be  $N$  vortex pairs as just described. Superimposing the  $N$  vortex pairs onto the cylinder in a uniform free stream flow, the stream and potential functions become:

$$\begin{aligned} \psi = U_{\infty} (Y \cos \alpha - X \sin \alpha) \left[ 1 - \frac{a^2}{X^2 + Y^2} \right] \\ + \sum_{i=1}^N \frac{\Gamma_i}{4\pi} \ln \left[ \frac{(X-A)^2 + (Y-B)^2}{(X-\xi)^2 + (Y-\eta)^2} \right] \end{aligned} \quad (18)$$

$$\begin{aligned} \phi = U_{\infty} (X \cos \alpha + Y \sin \alpha) \left[ 1 + \frac{a^2}{X^2 + Y^2} \right] \\ + \sum_{i=1}^N \frac{\Gamma_i}{2\pi} \arctan \left[ \frac{(X-\xi_i)(Y-B_i) - (X-A_i)(Y-\eta_i)}{(Y-\eta_i)(Y-B_i) + (X-\xi_i)(X-A_i)} \right] \end{aligned} \quad (19)$$

The velocity at any point  $(X, Y)$  in the flow field can be obtained directly by differentiation and some algebraic

manipulation of Eq. (18). The velocities in the X-direction ( $U_0$ ) and the Y-direction ( $V_0$ ) are:

$$U_0 = \frac{\partial \psi}{\partial Y} = U_\infty \left[ \cos \alpha - \frac{a^2 \cos \alpha}{X^2 + Y^2} - \frac{2a^2 XY \sin \alpha}{(X^2 + Y^2)^2} + \frac{2a^2 Y^2 \cos \alpha}{(X^2 + Y^2)^2} \right] + \sum_{i=1}^N \frac{\Gamma_i}{2\pi} \left[ \frac{Y - B_i}{(X - A_i)^2 + (Y - B_i)^2} - \frac{Y - \eta_i}{(X - \xi_i)^2 + (Y - \eta_i)^2} \right] \quad (20)$$

$$V_0 = \frac{-\partial \psi}{\partial X} = U_\infty \left[ \sin \alpha - \frac{a^2 \sin \alpha}{X^2 + Y^2} - \frac{2a^2 XY \cos \alpha}{(X^2 + Y^2)^2} + \frac{2a^2 X^2 \sin \alpha}{(X^2 + Y^2)^2} \right] + \sum_{i=1}^N \frac{\Gamma_i}{2\pi} \left[ \frac{X - \xi_i}{(X - \xi_i)^2 + (Y - \eta_i)^2} - \frac{X - A_i}{(X - A_i)^2 + (Y - B_i)^2} \right]. \quad (21)$$

The stream function  $\psi$ , potential function  $\phi$ , and general velocities  $U_0$  and  $V_0$  for any point in the  $\rho$ -plane are now known.

### Joukowski Transformation

The Joukowski transformation can be used to transform a flow from a cylinder plane to an airfoil plane. We already have the equations for the flow in the  $\rho$ -plane, where the cylinder is centered at the origin. In complex variable form, the position of a point in the  $\rho$ -plane can be expressed as  $\rho = r e^{i\theta}$ . We can transform this point to the  $\rho'$ -plane by the transformation  $\rho' = \rho e^{-i\beta} + \mu$  (10:461). This rotates points in the  $\rho$ -plane  $\beta$  radians clockwise, and then

displaces them by an amount  $\mu$ . The positive X-coordinate crossed by the cylinder in the  $\rho$ -plane,  $\rho_t$ , maps into the point  $\rho_t'$  (see Fig. 2). Transforming from the  $\rho'$ -plane to the Z-plane, the Joukowski transformation is used. It is given by:

$$Z = \rho' + \frac{\rho_t'^2}{\rho'} \quad (22)$$

This transforms the cylinder in the  $\rho'$ -plane to an airfoil shape in the Z-plane. The point  $\rho_t'$  maps to the trailing edge of the airfoil shape in the Z-plane.

#### Determination of Strength of Vortices

Having seen how the Joukowski transformation maps a cylinder in the  $\rho$ -plane into an airfoil shape in the Z-plane, it is time to relate the flows in the  $\rho$  and Z-planes. As mentioned before, the solution involves placing discrete vortices in the airfoil wake to simulate the vortex sheet shed into the wake as circulation builds around the airfoil. Images of these vortices are placed inside the cylinder to simulate the airfoil bound vortex. The strength of each vortex is determined by satisfying the Kutta condition at each discrete time step. The Kutta condition implies that a stagnation point of the flow is at the airfoil trailing edge. As seen in the Joukowski transformation, the point  $\rho_t$  in the  $\rho$ -plane maps into the trailing edge of the airfoil in the Z-plane. Therefore, establishing a stagnation point at  $\rho_t$  in the  $\rho$ -plane satisfies the Kutta condition in the Z-plane (10:469).



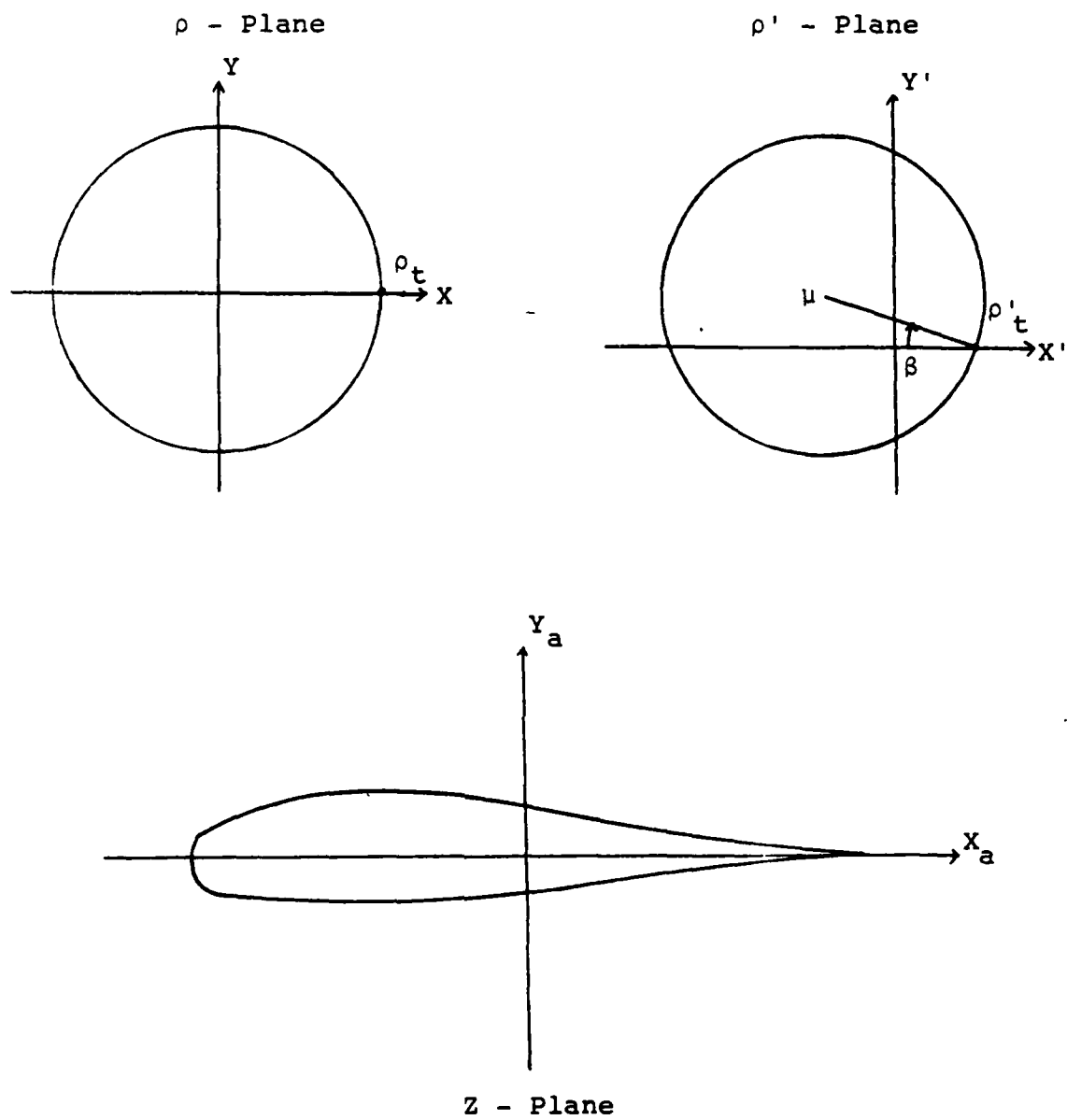


Fig. 2. Planes of the Joukowski Transformation

To make  $o_t$  a stagnation point in the  $o$ -plane, set the velocity  $U_o$  equal to zero at that point and solve for the circulation strength  $\Gamma$  in Eq. (20). This value of  $\Gamma$  will be the same in the  $Z$ -plane, for circulation is unchanged in the Joukowski transformation (10:458). Taking Eq. (20) for  $U_o$ , letting the cylinder radius  $a = 1$ , and recalling that  $X^2 + Y^2 = 1$  for points on a cylinder of radius  $a = 1$ , one arrives at:

$$U_o = 0 = U_\infty \left[ \cos \alpha - \cos \alpha - 2XY \sin \alpha + 2Y^2 \cos \alpha \right] + \sum_{i=1}^N \frac{\Gamma_i}{2\pi} \left[ \frac{Y-B_i}{(X-A_i)^2 + (Y-B_i)^2} - \frac{Y-\eta_i}{(X-\xi_i)^2 + (Y-\eta_i)^2} \right] \quad (23)$$

Let  $N = 1$  to solve for the strength of the first shed vortex. Solving for  $\Gamma/U_\infty$ , one gets:

$$\frac{\Gamma}{U_\infty} = \frac{2\pi (2XY \sin \alpha - 2Y^2 \cos \alpha)}{\left[ \frac{Y-B}{(X-A)^2 + (Y-B)^2} - \frac{Y-\eta}{(X-\xi)^2 + (Y-\eta)^2} \right]} \quad (24)$$

Recalling the relations for  $A$  and  $B$  given by Eqs. (13) and (14) and again making use of the fact that  $X^2 + Y^2 = 1$  on the cylinder, Eq. (24) becomes

$$\frac{\Gamma}{U_\infty} = \frac{4\pi (X \sin \alpha - Y \cos \alpha) (\xi^2 + \eta^2 + 1 - 2(X\xi + Y\eta))}{\xi^2 + \eta^2 - 1} \quad (25)$$

Define  $\Gamma/U_\infty$  as  $\Gamma^*$ , the non-dimensional circulation, and note that at  $o_t$ ,  $X = 1$  and  $Y = 0$ . This changes Eq. (25) to

$$\Gamma^* = \frac{4\pi \sin \alpha (\xi^2 + \eta^2 + 1 - 2\xi)}{\xi^2 + \eta^2 - 1} \quad (26)$$

When solving for each subsequent  $\Gamma^*$  term, all previous  $\Gamma^*$  terms are known. Thus, Eq. (23) can be solved for  $\Gamma_i^*$ .

In general, then

$$\Gamma_i^* = \frac{4\pi \sin \alpha_i (\xi_i^2 + \eta_i^2 + 1 - 2\xi_i)}{\xi_i^2 + \eta_i^2 - 1} - \sum_{k=1}^{i-1} \frac{\Gamma_k^* (\xi_k^2 + \eta_k^2 - 1)}{\xi_k^2 + \eta_k^2 + 1 - 2\xi_k} \quad (27)$$

#### Velocities Induced at Discrete Vortices and on the Cylinder

For each time step taken, the strength of the vortex pair introduced at that time step can now be calculated using Eq. (27). However, from one time step to the next, each vortex introduced in the wake moves away from the airfoil some distance, that distance being equal to the velocity at the position of the vortex times the time step,  $\Delta t$ . The velocity at the position of each vortex depends upon not only the free stream velocity, but also the velocities induced at that position by all other vortices in the field. Equations (20) and (21) can be used to find that velocity in the  $\rho$ -plane. Let  $(\xi_m, \eta_m)$  be the coordinates of the position at which the trailing vortex is located, the  $i$  subscript denote the time step at which the velocity is computed, and the  $k$  subscript identify an individual vortex.

Solving equations (20) and (21) for the non-dimensional  $U_m/U_\infty$ ,  $V_m/U_\infty$ , and recalling  $\Gamma_m^* = \Gamma_m/U_\infty$ , one gets:

$$\frac{U_m}{U_\infty} = \cos \alpha_i - \frac{\cos \alpha_i}{\xi_m^2 + \eta_m^2} - \frac{2\xi_m \eta_m \sin \alpha_i}{(\xi_m^2 + \eta_m^2)^2} + \frac{2\eta_m^2 \cos \alpha_i}{(\xi_m^2 + \eta_m^2)^2} + \frac{\Gamma_m^*}{2\pi} \left[ \frac{\eta_m(\xi_m^2 + \eta_m^2 - 1)}{(\xi_m^2 + \eta_m^2)^2 - 2\xi_m^2 - 2\eta_m^2 + 1} \right] \quad (28)$$

$$+ \sum_{\substack{k=1, \\ k \neq m}}^N \frac{\Gamma_k^*}{2\pi} \left[ \frac{\eta_m^{-B_k}}{(\xi_m^{-A_k})^2 + (\eta_m^{-B_k})^2} - \frac{\eta_m^{-\eta_k}}{(\xi_m^{-\xi_k})^2 + (\eta_m^{-\eta_k})^2} \right]$$

$$\frac{V_m}{U_\infty} = \sin \alpha_i - \frac{\sin \alpha_i}{\xi_m^2 + \eta_m^2} - \frac{2\xi_m \eta_m \cos \alpha_i}{(\xi_m^2 + \eta_m^2)^2} + \frac{2\xi_m^2 \sin \alpha_i}{(\xi_m^2 + \eta_m^2)^2} - \frac{\Gamma_m^*}{2\pi} \left[ \frac{\xi_m(\xi_m^2 + \eta_m^2 - 1)}{(\xi_m^2 + \eta_m^2)^2 - 2\xi_m^2 - 2\eta_m^2 + 1} \right] \quad (29)$$

$$+ \sum_{\substack{k=1, \\ k \neq m}}^N \frac{\Gamma_k^*}{2\pi} \left[ \frac{\xi_m^{-\xi_k}}{(\xi_m^{-\xi_k})^2 + (\eta_m^{-\eta_k})^2} - \frac{\xi_m^{-A_k}}{(\xi_m^{-A_k})^2 + (\eta_m^{-B_k})^2} \right]$$

Equations (28) and (29) describe the velocity that exists at any vortex location  $(\xi_m, \eta_m)$  as induced by the uniform free stream and all other vortices in the flow field.

The velocity induced along the cylinder surface is needed to determine the pressure distribution on the airfoil. Again making use of the  $o$ -plane velocity equations (20) and (21), and recalling that  $X^2 + Y^2 = 1$  on the cylinder in the  $o$ -plane, the non-dimensional velocities become:

$$\frac{U}{U_\infty} = -2XY \sin \alpha + 2Y^2 \cos \alpha + \sum_{i=1}^N \frac{\Gamma_i^*}{2\pi} \left[ \frac{Y(\xi_i^2 + \eta_i^2 - 1)}{\xi_i^2 + \eta_i^2 - 2(X\xi_i + Y\eta_i) + 1} \right] \quad (30)$$

$$\frac{V}{U_\infty} = -2XY \cos \alpha + 2X^2 \sin \alpha - \sum_{i=1}^N \frac{\Gamma_i^*}{2\pi} \left[ \frac{X(\xi_i^2 + \eta_i^2 - 1)}{\xi_i^2 + \eta_i^2 - 2(X\xi_i + Y\eta_i) + 1} \right] \quad (31)$$

where  $(X, Y)$  are coordinates of a point on the cylinder surface. In the  $o$ -plane, these points can be easily put into cylindrical coordinates. Let  $X = r \cos \theta$ ,  $Y = r \sin \theta$ , where  $r = 1$ , the radius of the cylinder. Equations (30) and (31) then become:

$$\frac{U}{U_\infty} = -2 \cos \theta \sin \theta \sin \alpha + 2 \sin^2 \theta \cos \alpha + \sum_{i=1}^N \frac{\Gamma_i^*}{2\pi} \left[ \frac{\sin \theta (\xi_i^2 + \eta_i^2 - 1)}{\xi_i^2 + \eta_i^2 - 2(\xi_i \cos \theta + \eta_i \sin \theta) + 1} \right] \quad (32)$$

$$\frac{v}{U_\infty} = -2 \cos \theta \sin \theta \cos \alpha + 2 \cos^2 \theta \sin \alpha + \sum_{i=1}^N \frac{\Gamma_i^*}{2\pi} \left[ \frac{\cos \theta (\xi_i^2 + \eta_i^2 - 1)}{\xi_i^2 + \eta_i^2 - 2(\xi_i \cos \theta + \eta_i \sin \theta) + 1} \right] \quad (33)$$

Since the cylinder surface is a streamline of the flow, the velocity on the cylinder is always parallel to the surface. Therefore, the magnitude of the non-dimensional velocity tangent to the surface of the cylinder,  $U_\theta$ , is just:

$$U_\theta = \left[ \left( \frac{U}{U_\infty} \right)^2 + \left( \frac{v}{U_\infty} \right)^2 \right]^{1/2} \quad (34)$$

#### Circulation About the Airfoil

As the wake behind the airfoil forms, circulation develops about the airfoil in the form of a bound vortex. The strength of this bound vortex defines the total circulation about the airfoil. Since the value of the total circulation in the flow field must be zero, then the strength of the circulation about the airfoil must be equal in magnitude and opposite in sign to the total circulation in the wake. The circulation in the wake is just the sum of the strengths of all the discrete vortices in the wake. The circulation can be calculated by

$$\Gamma_a^* = \sum_{i=1}^N -\Gamma_i^* \quad (35)$$

where  $\Gamma_a^*$  is the non-dimensional circulation about the airfoil,  $\Gamma_i^*$  is as defined in Eq. (27), and N is the number of discrete vortices in the wake.

### Velocity in the Airfoil Frame

Now that expressions for velocities in the  $\rho$ -plane are known (Eqs. (32), (33) and (34)), their values at corresponding points in the Z-plane can be found. Consider the complex potential  $F(\rho) = \phi + i\psi$ , where  $\rho = X + iY$  in the  $\rho$ -plane. The complex velocity in the  $\rho$ -plane is  $dF/d\rho = w(\rho)$ . Since  $\rho' = \rho e^{-i\beta} + \mu$ , then  $\rho'$  is a function of  $\rho$ . By the chain rule of differentiation,  $dF/d\rho = (dF/d\rho')(d\rho'/d\rho)$ , where  $dF/d\rho' = w(\rho')$ , the complex velocity in the  $\rho'$ -plane. Therefore

$$w(\rho') = w(\rho) \cdot \frac{1}{\frac{d\rho'}{d\rho}} \quad (36)$$

Note that the magnitude of  $d\rho'/d\rho = 1$ , and thus the magnitude of the complex velocity in the  $\rho$ -plane equals the magnitude of the complex velocity at the corresponding point in the  $\rho'$ -plane. By similar arguments, knowing that the transformation from the  $\rho'$ -plane to the Z-plane is given by Eq. (22), and using the chain rule once more, it can be shown that

$$U_Z - iV_Z = w(Z) = w(\rho') \cdot \frac{1}{\frac{dZ}{d\rho'}} = w(\rho) \cdot \frac{1}{\frac{dZ}{d\rho}} \quad (37)$$

In this case

$$\frac{dz}{d\phi'} = 1 - \frac{c_t^2}{(\phi')^2} \quad (38)$$

Thus, given the magnitude of a velocity at a point in the  $\phi$ -plane, the magnitude of the velocity at the corresponding point in the  $Z$ -plane can be found using Eq. (37).

All the tools needed to analyze the airfoil wake effects are now known. The stream and potential functions in the  $\phi$ -plane are known, from which velocities in the  $\phi$ -plane can be found. The strength  $\Gamma^*$  of the wake vortices and their images can be found by requiring the stagnation point in the  $\phi$ -plane to remain fixed, thus satisfying the Kutta condition on the airfoil in the  $Z$ -plane. The values of  $\Gamma^*$  are the same in both planes, and velocities in the  $\phi$ -plane can be directly transformed to the  $Z$ -plane.

#### Pressure, Lift, Vorticity Distribution on the Airfoil

The unsteady Bernoulli equation is used to calculate the pressure on the airfoil. It is given by (6:18)

$$P + \frac{1}{2} \rho U^2 + \rho \frac{\partial \phi}{\partial t} = \rho f(t) \quad (39)$$

where  $P$  is pressure,  $\rho$  is the fluid density,  $U$  is the fluid velocity,  $\phi$  is the potential function, and  $f(t)$  is a function of time independent of position. The subscripts  $l$  and  $u$  will be used to denote the lower and upper surfaces of the airfoil, respectively. Subtracting the pressure on the upper surface from the pressure on the lower surface yields



$$P_l - P_u = \frac{1}{2} \rho (U_u^2 - U_l^2) + \rho \frac{\partial}{\partial t} (\phi_u - \phi_l) \quad (40)$$

The velocities in Eq. (40) are those tangent to the airfoil surface. Along a streamline,  $U = \partial\phi/\partial S$ , where  $S$  is the coordinate along the streamline. This implies that  $\phi = \int U ds$ . Therefore,

$$P_l - P_u = \frac{1}{2} \rho (U_u^2 - U_l^2) + \rho \frac{\partial}{\partial t} \int_{-\infty}^{S_a} (U_u - U_l) ds \quad (41)$$

Integrating in Eq. (41) from  $-\infty$  to  $S_a$ , the point on the streamline where  $P$ ,  $U_u$  and  $U_l$  are known or desired, one finds that the integral is zero from  $-\infty$  to  $-\frac{1}{2}c$ , the airfoil leading edge. Equation (41) then becomes

$$P_l - P_u = \frac{1}{2} \rho (U_u^2 - U_l^2) + \rho \frac{\partial}{\partial t} \int_{-\frac{1}{2}c}^{S_a} (U_u - U_l) ds \quad (42)$$

Introduce the following non-dimensional variables, identified by the superscript  $*$ :

$$t^* = \frac{t U_\infty}{\frac{1}{2}c}, \quad U^* = \frac{U}{U_\infty}, \quad S^* = \frac{S}{\frac{1}{2}c} \quad (43)$$

Equation (42) now becomes:

$$P_l - P_u = \frac{1}{2} \rho U_\infty^2 (U_u^{*2} - U_l^{*2}) + \rho U_\infty^2 \frac{\partial}{\partial t^*} \int_{-1}^{S_a^*} (U_u^* - U_l^*) ds^* \quad (44)$$

Recall the definition of the coefficient of pressure  $C_p = (P - P_\infty) / \frac{1}{2} \rho U_\infty^2$ . The difference between the coefficients of pressure on the lower and upper airfoil surface is called  $\Delta C_p$ . Using this definition, one obtains from Eq. (44)

$$\frac{P_u - P_l}{\frac{1}{2} \rho U_\infty^2} = -\Delta C_p = U_u^{*2} - U_l^{*2} + 2 \frac{\partial}{\partial t^*} \int_{-1}^1 S_a^* (U_u^* - U_l^*) ds^* \quad (45)$$

The coefficient of lift per unit span,  $C_l$ , is defined as  $C_l = L / \frac{1}{2} \rho U_\infty^2 c$ , where  $L$  is the lift per unit span and  $c$  is the chord. Since  $L$  is defined as  $\int_{-\frac{1}{2}c}^{\frac{1}{2}c} \Delta P dx$ , and  $\Delta P = -\Delta C_p \cdot \frac{1}{2} \rho U_\infty^2$ , then

$$C_l = \int_{-\frac{1}{2}c}^{\frac{1}{2}c} -\frac{\Delta C_p}{c} dx \quad (46)$$

where  $X$  is measured along the chord of the airfoil.

The non-dimensional vorticity,  $\gamma^*$ , is defined as  $U_u^* - U_l^*$ . The vorticity distribution can be easily calculated using this relation, since the value of  $\gamma^*$  can be obtained directly for any position along the airfoil chord where the velocities on the upper and lower surfaces of the airfoil are known.

#### Numerical Solution Process

The following procedure is used to numerically analyze the wake vortex effects on the airfoil.

Step 1 - Select a non-dimensional time step  $\Delta t^*$ , defined as  $\Delta t^* = \Delta t U_\infty / (\frac{1}{2}c)$ . Let the airfoil begin its motion at an initial angle of attack  $\alpha_0$  and velocity  $U_\infty$ . Assume that after a time  $\Delta t^*$ , at time  $i = 1$ , the first shed vortex is at a position  $U_\infty \Delta t$  downstream of the airfoil trailing edge in the direction of the velocity at the trailing edge.

Step 2 - The first vortex is thus at  $(\xi, \eta)$  in the  $o$ -plane, and Eq. (26) can be solved for  $\Gamma^*$ . The circulation about the airfoil is  $-\Gamma^*$ .

Step 3 - Eqs. (32), (33) and (34) can now be solved for the velocity in the  $o$ -plane at any point  $(X, Y)$  on the cylinder. These velocities can be transformed to the  $Z$ -plane by Eq. (37).

Step 4 - Eq. (45) can be solved for  $\Delta C_p$  using a trapezoidal rule with variable  $\Delta X$  for the integration along the upper and lower surfaces of the airfoil, and a three-point backward difference differentiation approximation for the derivative with respect to time. (For steps  $i = 1$  and  $i = 2$ , a two-point linear difference method is used for the time derivative.) Eq. (46) can then be solved for  $C_\ell$ , again using a trapezoidal rule with variable  $\Delta X$  for the integration. The non-dimensional vorticity distribution can be calculated directly as  $\gamma^* = U_u^* - U_\ell^*$ .

Step 5 - The velocity of the shed vortex is calculated using Eqs. (28), (29) and (37). For the next time step, the vortex has moved in the  $Z$ -plane by an amount  $U_{SV}^* \Delta t^*$ , where  $U_{SV}^*$  is the non-dimensional velocity of the vortex just calculated. Its position in the  $o$ -plane is then determined by the inverse Joukowski transformation, given by

$$o = \left[ \frac{Z \pm (Z^2 - 4o_t^2)^{1/2} - \mu}{2} \right] e^{i\beta} \quad (47)$$

where only the plus sign of the  $\pm$  term gives a value of  $o$  in the wake, and thus it is the value used for  $o$ .

Step 6 - For the next time step,  $i = 2$ , the vortex shed at time  $i = 1$  is at the position computed in step 5. Assume the vortex shed at time  $i = 2$  is at the position  $U_\infty \Delta t$  downstream of the trailing edge. The angle of attack at  $i = 2$  is now  $\alpha_0 + \dot{\alpha}^* \Delta t^*$ , where  $\dot{\alpha}^*$  is defined as

$$\dot{\alpha}^* = \frac{\dot{\alpha} \frac{1}{2} c}{U_\infty} \quad (48)$$

Step 7 - All terms in Eq. (27) are now known, and this equation can be solved for  $\Gamma_2^*$ . The circulation about the airfoil is  $-(\Gamma_1^* + \Gamma_2^*)$ .

Step 8 - Eqs. (32), (33) and (34) can be solved for the velocity on the cylinder in the  $o$ -plane, and then the velocities can be expressed in the  $Z$ -plane using Eq. (37).

Step 9 - The values of  $\Delta C_p$  and  $C_l$  can be found using Eqs. (45) and (46) respectively, and the vorticity distribution  $\gamma^*$  is again just  $U_u^* - U_l^*$ .

Step 10 - The velocity at the shed vortices can be calculated using Eqs. (28), (29) and (37). The vortices are then moved in the  $Z$ -plane a distance  $U_{SV}^* \Delta t^*$ . This new position of each vortex in the  $Z$ -plane is the assumed location of each vortex for the next time step. Each vortex position in the  $o$ -plane can be determined by using the inverse Joukowski transformation, Eq. (47).

Step 11 - For each time step  $i$ , the position of each vortex is known from time step  $i - 1$ , and the vortex shed at time  $i$  is assumed to be a distance  $U_\infty \Delta t$  downstream of the trailing edge in the direction of the velocity at the

trailing edge. The angle of attack  $\alpha$  at time step  $i$  is  $\alpha_i = \alpha_{i-1} + \dot{\alpha}^* \Delta t^*$ . Eqs. (27), (35), (32), (33), (34), (37), (45) and (46) are then used to compute  $\Gamma_i^*$ , airfoil circulation, velocities on the airfoil,  $\Delta C_p$  and  $C_l$  for time step  $i$ . Eqs. (28), (29) and (37) are used to find the position of the shed vortices for time step  $i + 1$ .

Step 11 is repeated as often as desired to compute the airfoil circulation, pressure difference distribution, coefficient of lift,  $\gamma$  distribution, and shed vortex positions for any discrete time desired.

### III. Results

#### Numerical Method Verification

Before exploring the effect of a constant- $\dot{\alpha}$  flow on the production of lift on a Joukowski airfoil, the method developed here was compared to the results of others. The first test case was that of a flat plate impulsively started at an infinitesimal angle of attack,  $\alpha$ . This problem was first explored by Wagner (11) in 1925. Wagner assumed in his analysis that the wake vortex sheet remained along the  $x_a$ -axis at all times. For infinitesimal  $\alpha$ , this is a good approximation. In Figs. 3 and 4 a numerical computation for a flat plate in the Z-plane, impulsively started at  $\alpha = 0.01$  radians,  $\Delta t^* = 0.02$ , is compared with Wagner's analytic results and Giesing's (12) numerical results. The horizontal axis scale is  $U_\infty \Delta t / \frac{1}{2}c$ , which is the non-dimensional distance the airfoil has traveled since the motion started, having a value of one for each half-chord distance of airfoil translation. The vertical scales,  $\Gamma / \Gamma_{ss}$  and  $C_l / C_{l_{ss}}$ , are the ratios of  $\Gamma$  or  $C_l$  to the steady-state values that would be obtained after a long period of time has passed, respectively. Both the build-up of circulation,  $\Gamma$  (Fig. 3), and the coefficient of lift,  $C_l$  (Fig. 4), closely approximate Wagner's curves.

In 1977, Shung (6) developed a numerical method similar to the one presented in this thesis, but limited the study to that for a flat plate at a constant  $\alpha$ . Unlike Wagner,

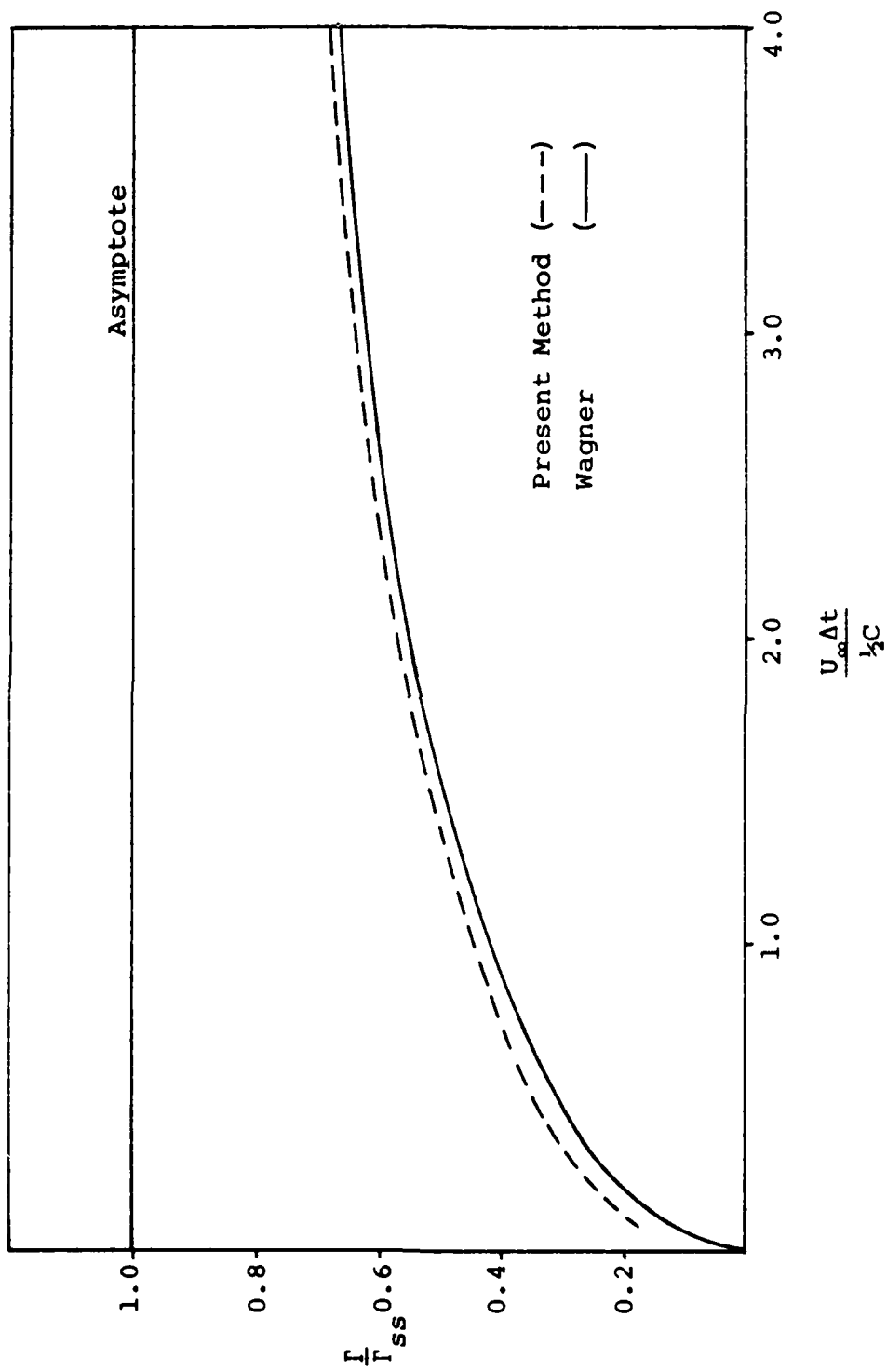


Fig. 3. Build-up of Circulation on an Impulsively-Started Flat Plate

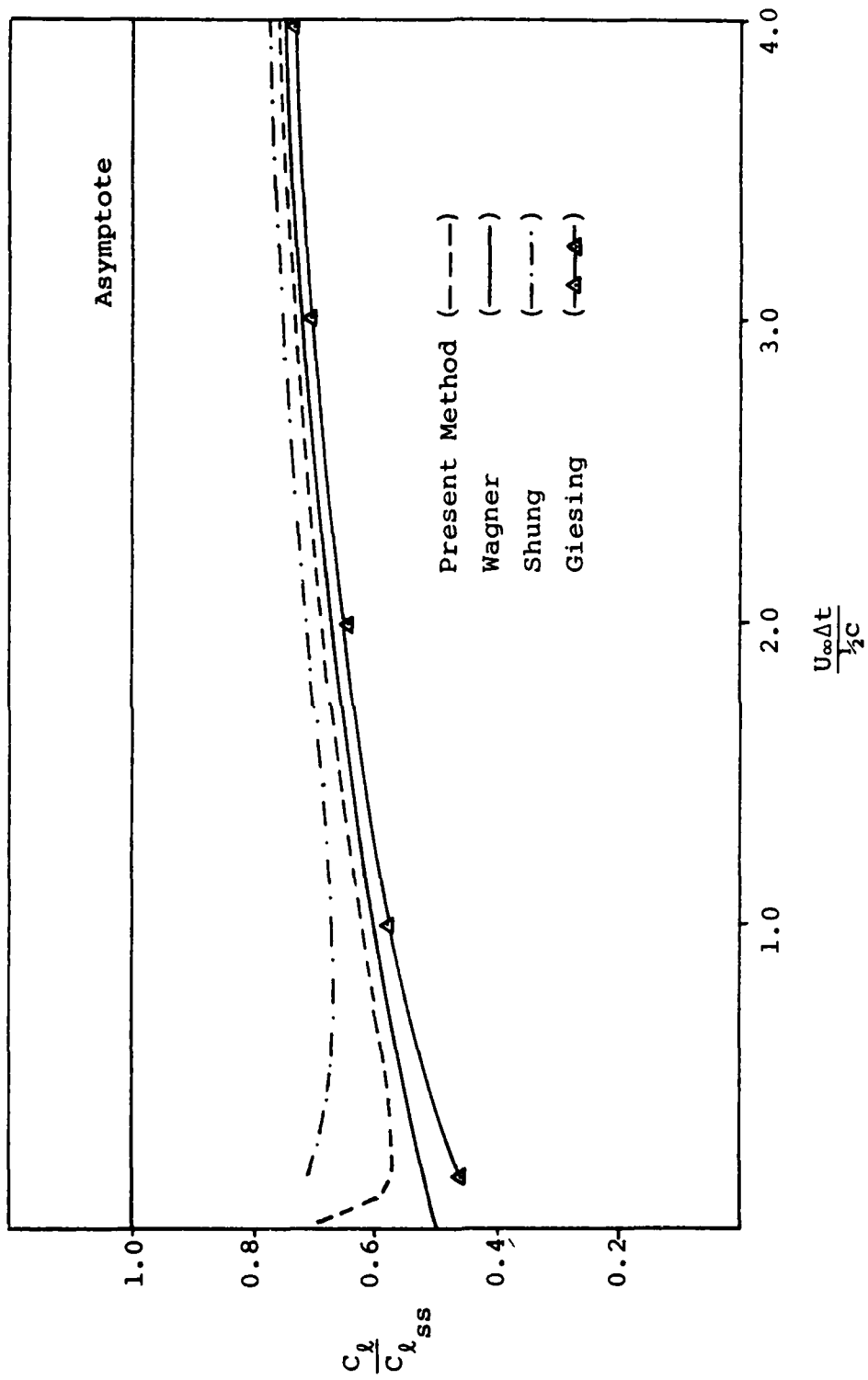


Fig. 4. Build-up of  $C_l$  on an Impulsively-Started Flat Plate



however, Shung's method allowed for vortex interactions in the airfoil wake, as does the method in this thesis. The major difference between Shung's numerical technique and the technique presented here lies in the method used to integrate the Unsteady Bernoulli Equation, Eq. (44). Since Shung was limited to a flat plate, he was able to integrate using the Gauss-Chebyshev quadrature formula (6:21). In this thesis, a trapezoidal rule with variable  $\Delta X$  was used for that integration. This allowed easy application to Joukowski airfoils. Figure 5 depicts  $C_l/C_{l_{ss}}$  for a flat plate at  $\alpha = 0.1$  radians at various values of  $\Delta t^*$ . Comparing the numerical solution with Wagner's curve, one sees that for smaller values of  $\Delta t^*$ , the numerical solution approaches Wagner's analytic solution. Shung (6:45) noted the same tendency with his numerical solution. Figure 6 depicts the formation of the vorticity distribution  $\gamma^*$  on a flat plate at  $\alpha = 0.1$  radians,  $\Delta t^* = 0.02$ . Note that immediately after the airfoil begins its motion, the vorticity is negative near the trailing edge, but as time passes, the vorticity distribution approaches that for the steady-state condition. Shung (6:44) showed the same effect in his study using  $\alpha = 0.1$  radians,  $\Delta t^* = 0.1$ . In fact, his results are identical to the results presented in Fig. 6. Similarly, the build-up to the steady-state pressure difference distribution for a flat plate at  $\alpha = 0.1$  radians can be seen in Fig. 7. Shung also demonstrated wake vortex sheet roll-up behind an impulsively-started flat plate. The method of

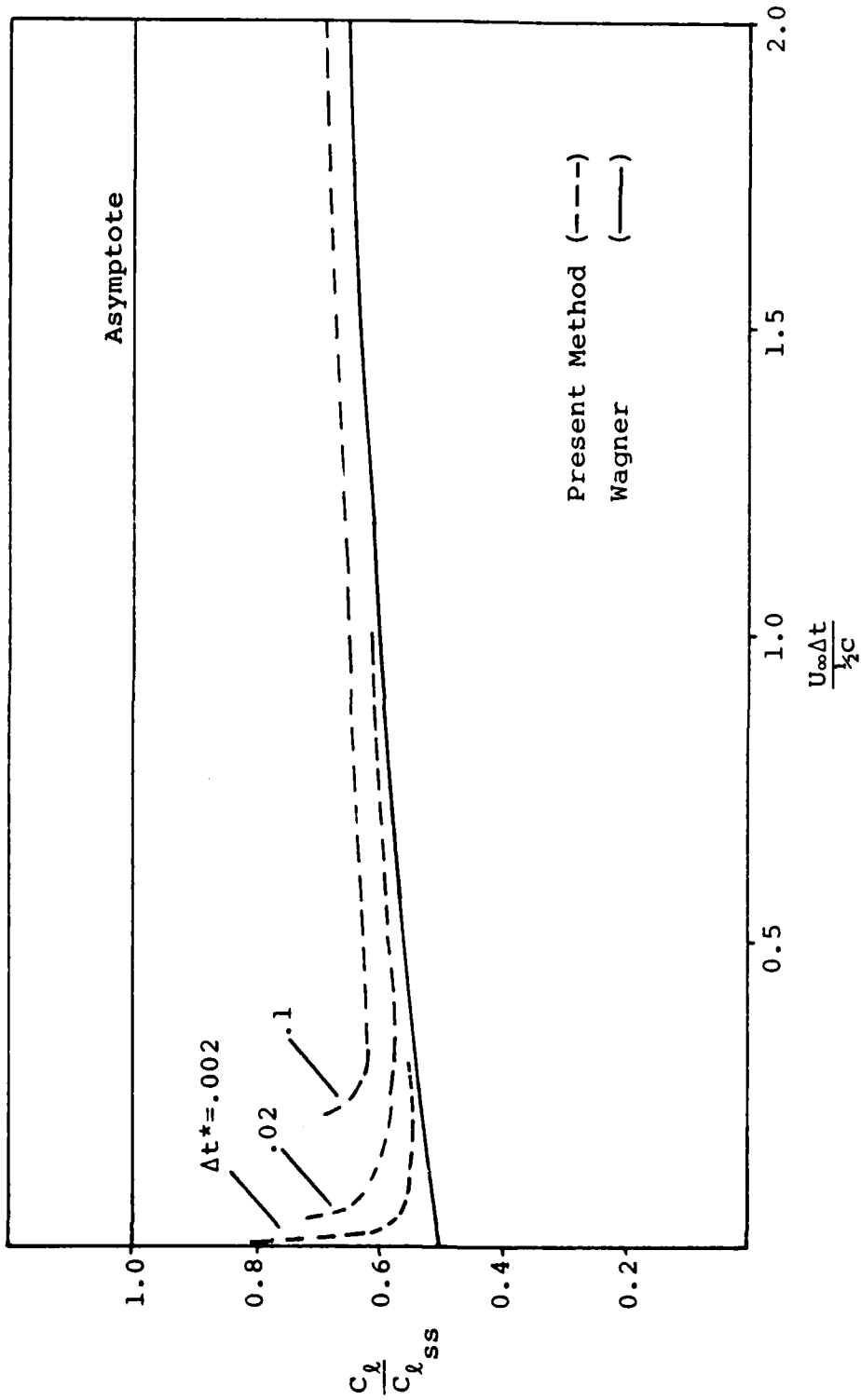


Fig. 5. Effect of  $\Delta t^*$  on Numerical Solution

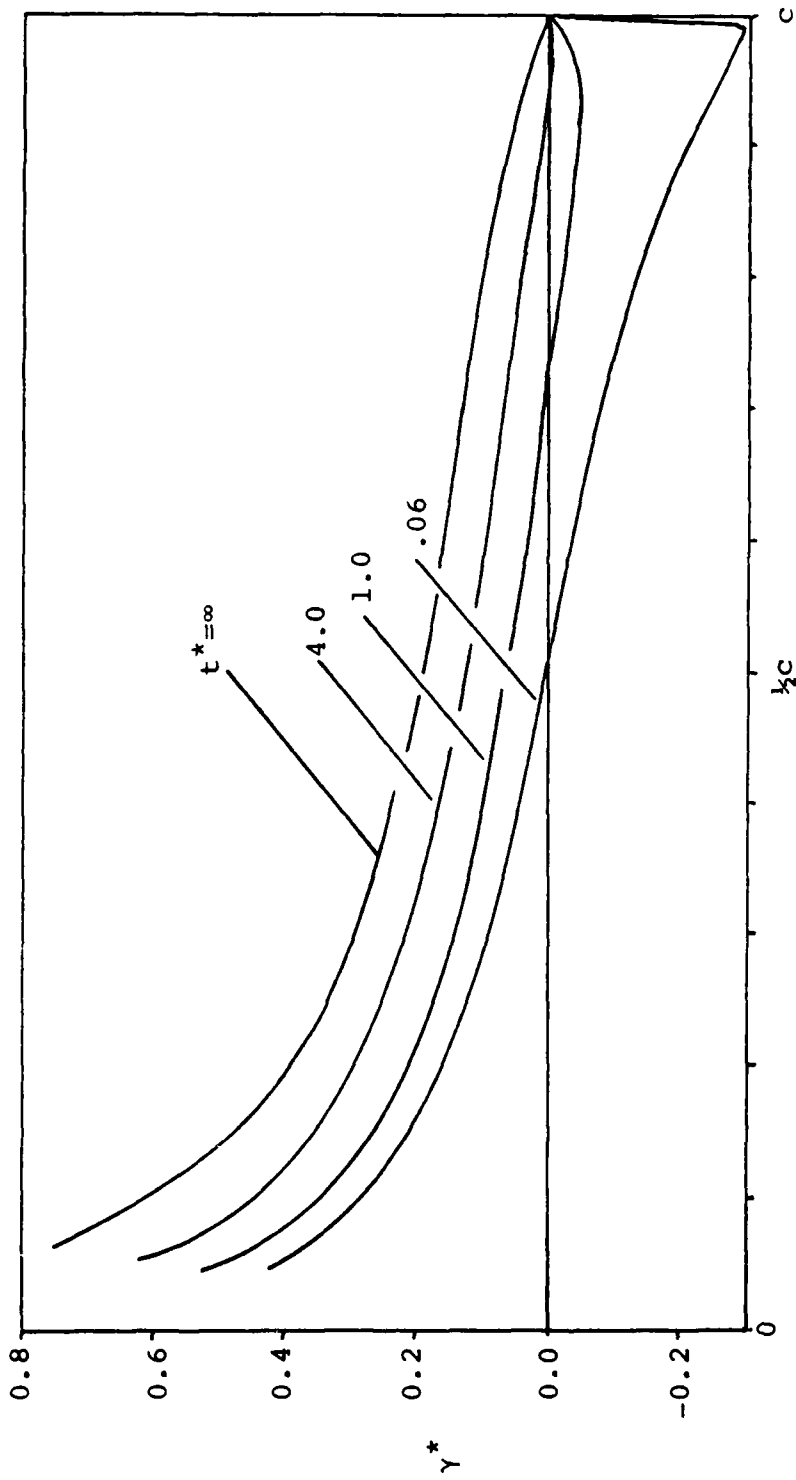


Fig. 6. Dimensionless Vorticity Distribution on a Flat Plate,  $\alpha=0.1$  Radians

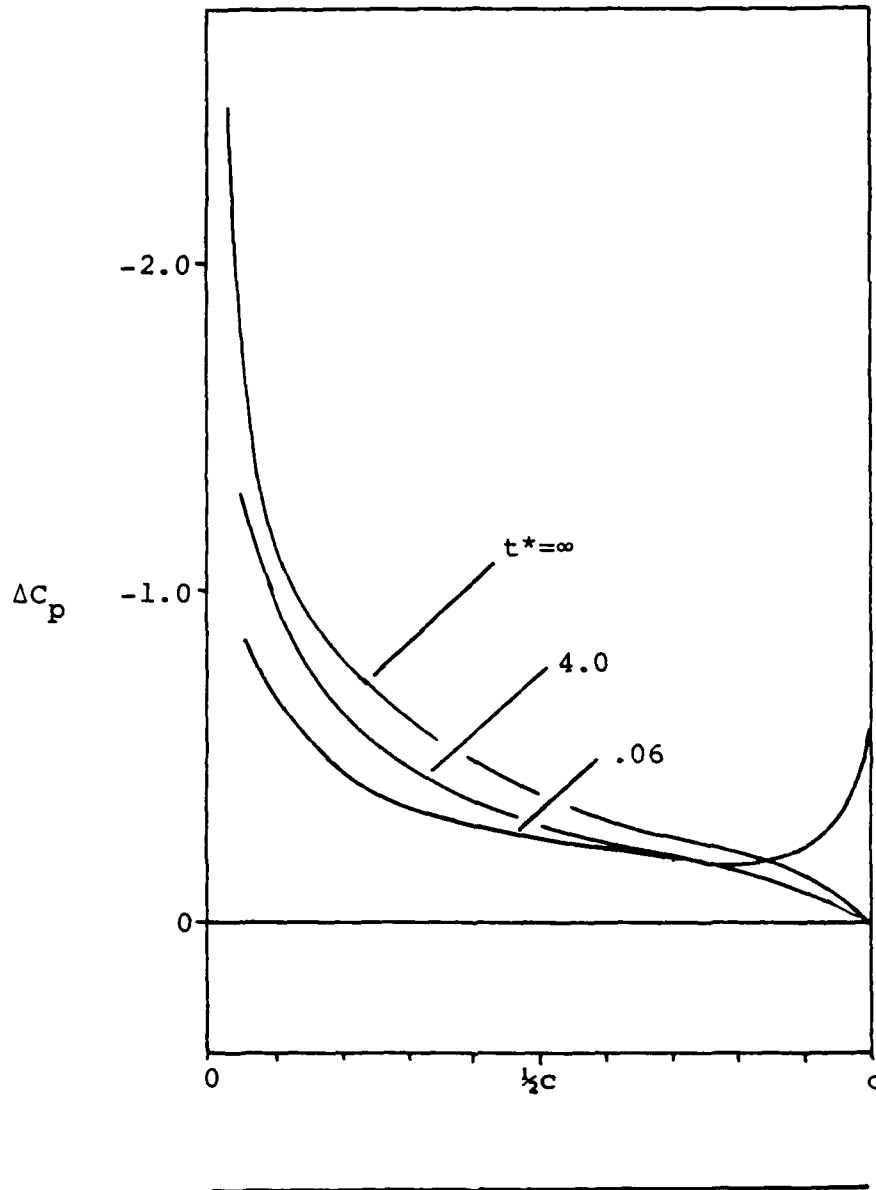


Fig. 7. Pressure Difference Distribution on a Flat Plate,  $\alpha=0.1$  Radians

this thesis demonstrates the same phenomenon, as can be seen in Fig. 8, which depicts wake vortex sheet roll-up for the case of an impulsively-started flat plate at  $\alpha = 0.1$  radians,  $\Delta t^* = 0.1$ , the same conditions depicted by Shung (6:43). Shung's depiction and Fig. 8 are almost identical.

The flat plate is, in fact, a special case of the more general Joukowski airfoil, and other airfoils in this family have been studied. Giesing (12) also developed a numerical procedure to account for wake effects on the build-up of lift on an arbitrary airfoil. Giesing published a curve of  $C_l/C_{l_{ss}}$  for a 25.5% thick symmetric Joukowski airfoil impulsively started at  $\alpha = 0.01$  radians. Using the same airfoil and motion conditions, a  $C_l/C_{l_{ss}}$  curve was developed using the numerical method presented in this thesis. Figure 9 compares those two curves with Wagner's curve for a flat plate. As can be seen in Fig. 4, Giesing's curve predicts values below those predicted by the present method. Whereas the present method over-predicted  $C_l$  for a flat plate, and Giesing's method under-predicted  $C_l$  for a flat plate, it seems likely that the ideal solution is bracketed by the present method and Giesing's method. Both curves for the 25.5% thick symmetric Joukowski airfoil show a greater delay in lift production than does the flat-plate-airfoil curve. This agrees with an analysis done by Chow, who showed that airfoils of increased thickness develop lift at a slower rate than thinner airfoils (13:14).

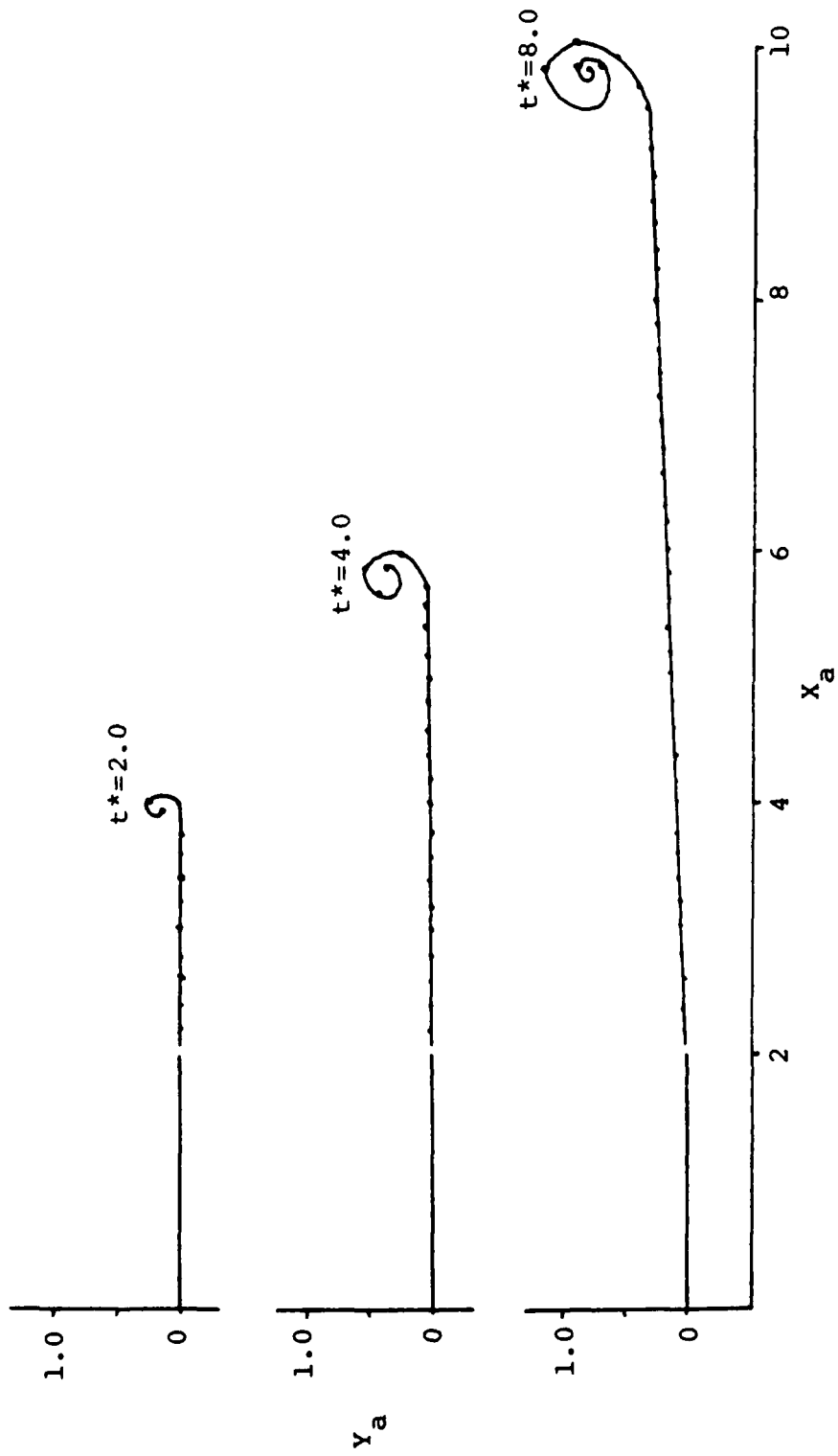


Fig. 8. Wake Vortex Sheet Roll-up For a Flat Plate,  $\alpha = 0.1$  Radians

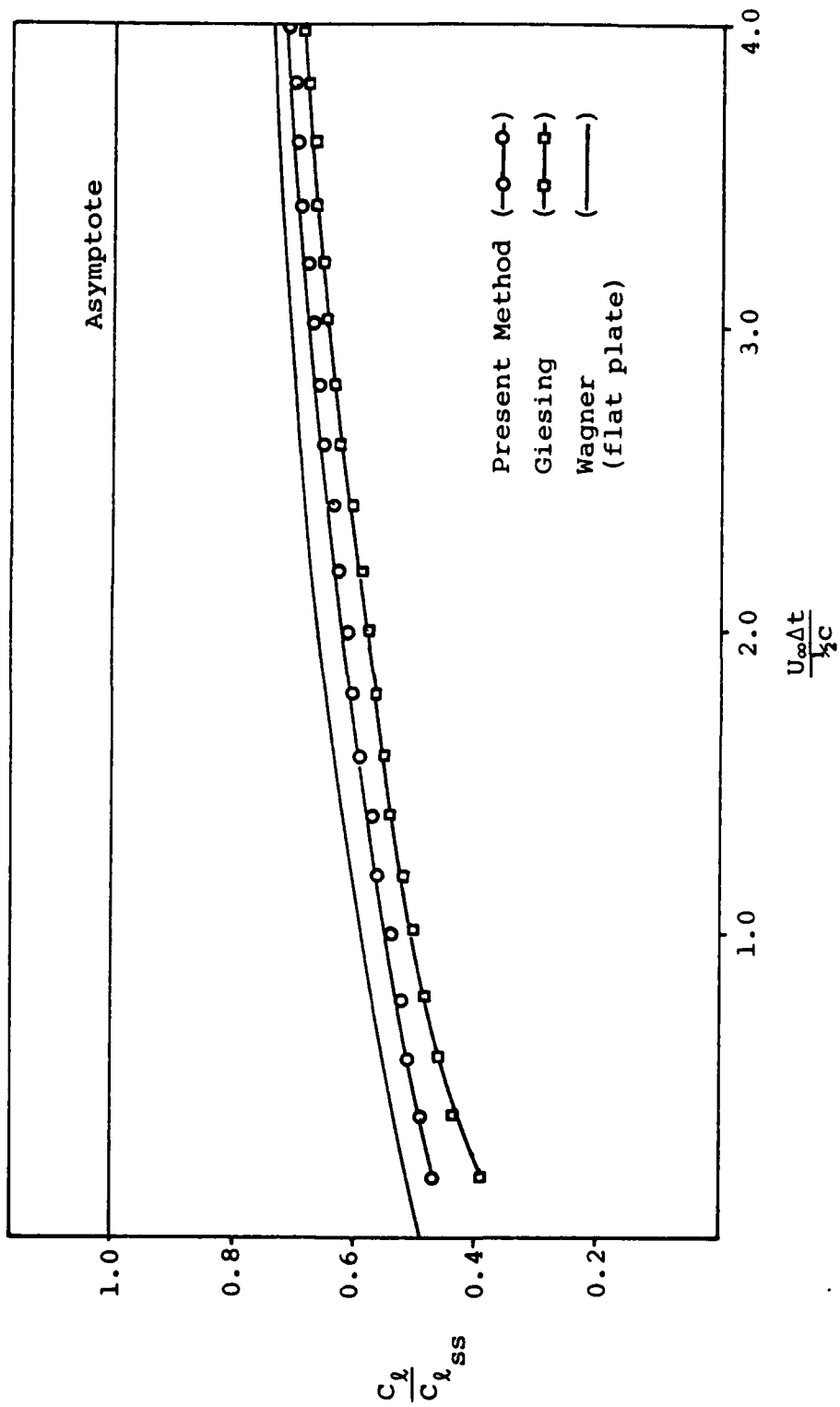


Fig. 9. Build-up of  $C_l$  on a 25.5% Thick Symmetric Joukowski Airfoil

Giesing's numerical technique and the one presented in this thesis differ in several ways. One major difference between the two numerical techniques is in the way the motion of the discrete vortices in the airfoil wake is predicted. In Giesing's technique, after each time step, the non-dimensional velocity induced at each trailing vortex position,  $U_o^*$ , is calculated and then multiplied by  $\Delta t^*$  to approximately predict where that discrete vortex will be at the next time step. The non-dimensional velocity induced at that predicted position,  $U_c^*$ , is then calculated. The average of  $U_o^* + U_c^*$  is then multiplied by  $\Delta t^*$  to correct the predicted position of each discrete vortex for the next time step. This method can be referred to as a Predictor-Corrector method. The numerical technique presented in this thesis predicts the discrete vortex position in the same manner as Giesing's predictor, but no corrector velocity is computed or used. The predicted velocity is the only velocity used to update vortex position.

To determine the effect a Predictor-Corrector method has on the numerical solution, a program incorporating Giesing's Predictor-Corrector method was developed. The results obtained using this program were compared with the results obtained using the method presented in this thesis for the same airfoil and conditions of motion. Figure 10 shows a comparison of wake shape as computed by the two methods for an impulsively started flat plate airfoil at  $\alpha = 10^\circ$ . Only in the area of starting vortex roll-up



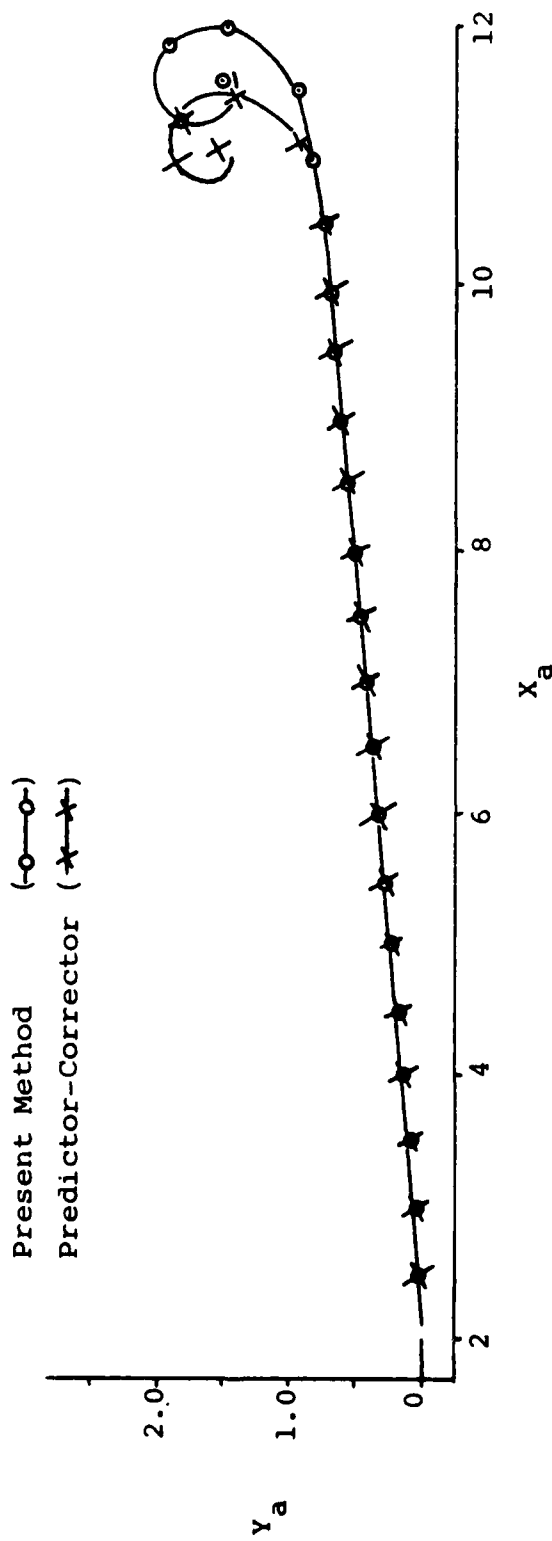


Fig. 10. Wake Vortex Sheet Roll-up for a Flat Plate,  $\alpha=10^\circ$

does the difference in vortex position become apparent. Further, the values of  $C_{\ell}/C_{\ell_{ss}}$  computed using the two methods are nearly identical, as seen in Table I. A comparison between the two methods was also made for the case of the flat plate initially at  $\alpha = 0^\circ$  subjected to an  $\dot{\alpha}^* = 0.035$ . One can see in Table II that the values of  $C_{\ell}/C_{\ell_{ss}}$  computed using the two methods are once again nearly identical. It was thus determined that the added computation time incurred by using the Predictor-Corrector method was not needed, and thus not included in other studies in this thesis.

As a final check of the method of this thesis, the development of  $\gamma^*$  and  $\Delta C_p$  on an impulsively-started symmetric airfoil with thickness was determined. Figures 11 and 12 show that for a 25.5% thick symmetric Joukowski airfoil impulsively started at  $\alpha = 0.1$  radians,  $\gamma^*$  and  $\Delta C_p$  build to their steady-state values in much the same manner as for a flat plate, Figs. 6 and 7, when using the numerical method of this thesis.

It has been shown that for the test cases above, the numerical method presented here is in good agreement with the work of others (6;11;12;13). There are two major advantages in using this numerical method over other methods. First, unlike Shung, one is not limited to a flat plate. Second, comparing to Giesing, the simpler method of vortex motion prediction greatly decreases computer run time while having a negligible effect on the prediction of lift build-up on an airfoil.

TABLE I

Comparison of  $C_l$  Calculated by Simple-Predictor Method to  $C_l$  Calculated by Predictor Corrector Method. Flat Plate Airfoil,  $\alpha = 10$

| $t^*$ | $C_l$  | Predictor-Corrector<br>$C_l$ |
|-------|--------|------------------------------|
| 1     | .70677 | .70779                       |
| 2     | .75962 | .75974                       |
| 3     | .79825 | .79827                       |
| 4     | .83271 | .83272                       |
| 5     | .85997 | .86000                       |
| 6     | .88199 | .88203                       |
| 7     | .90008 | .90010                       |
| 8     | .91515 | .91518                       |
| 9     | .92788 | .92789                       |
| 10    | .93873 | .93875                       |

TABLE II

Comparison of  $C_l$  Calculated by Simple-Predictor Method to  $C_l$  Calculated by Predictor Corrector Method. Flat Plate Airfoil,  $\alpha^* = 0.035$

| $t^*$ | $C_l$  | Predictor-Corrector<br>$C_l$ |
|-------|--------|------------------------------|
| 0.2   | .13710 | .13968                       |
| 0.4   | .16284 | .16543                       |
| 0.6   | .18888 | .19152                       |
| 0.8   | .21544 | .21814                       |
| 1.0   | .23061 | .23062                       |
| 1.2   | .27020 | .27301                       |
| 1.4   | .29837 | .30122                       |
| 1.6   | .32702 | .32991                       |
| 1.8   | .35612 | .35906                       |
| 2.0   | .38564 | .38863                       |

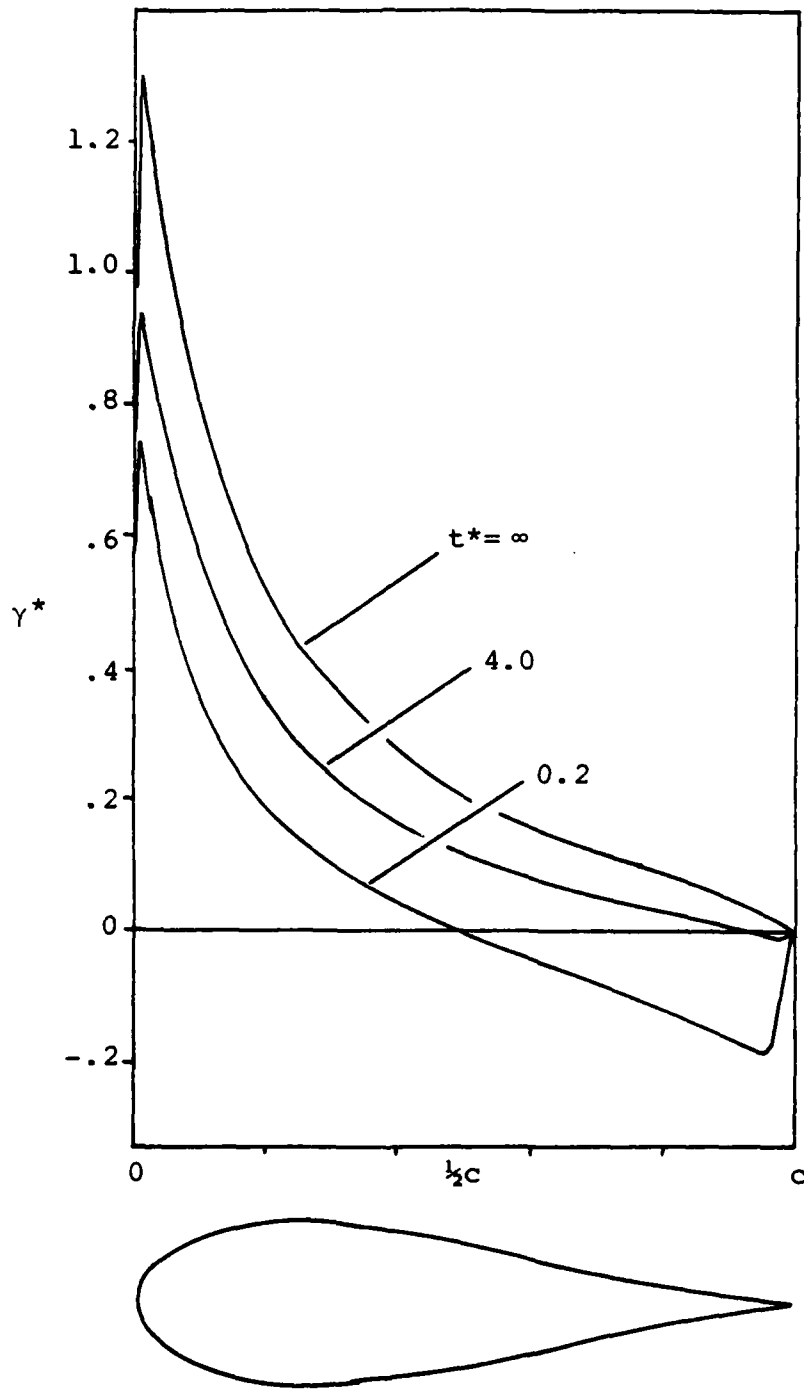


Fig. 11. Dimensionless Vorticity Distribution, 25.5% Thick Symmetric Joukowski Airfoil,  $\alpha=0.1$  Radians

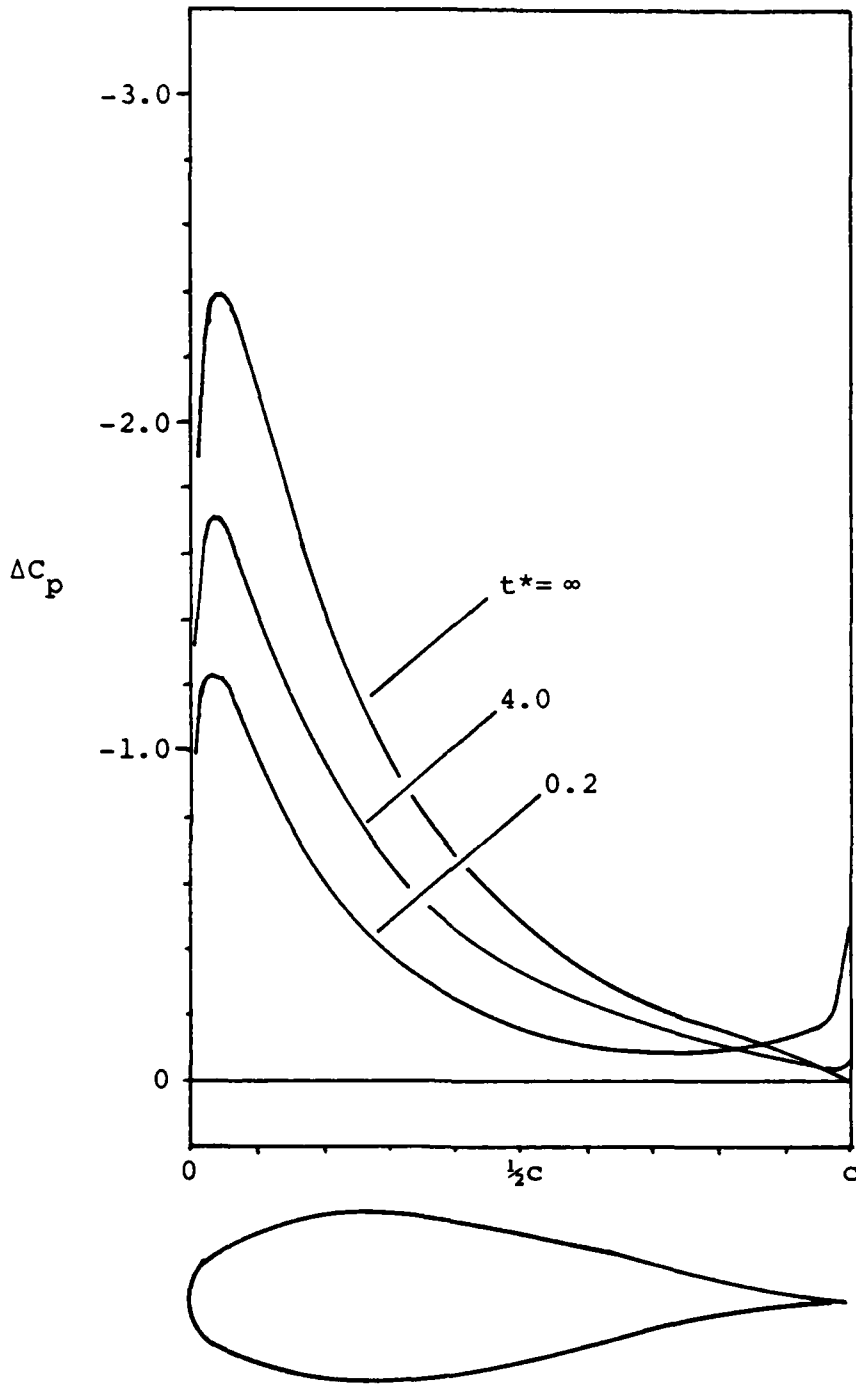


Fig. 12. Pressure Difference Distribution, 25.5% Thick Symmetric Joukowski Airfoil,  $\alpha=0.1$  Radians

### Application to Constant- $\dot{\alpha}$ Flow

In the last section it was shown that the present method compares favorably to the results of others for the constant- $\alpha$ , impulsively-started airfoil. In this section the results of applying the method to the previously-unstudied problem of constant- $\dot{\alpha}$  flow is presented. The presentation of these results is broken into four parts in order to more systematically explore and understand the interplay of possible effects. These four parts deal with the effects and selection of starting conditions, the general effect of  $\dot{\alpha}$  on the build-up of  $C_l$ , the effect of thickness, and the effect of camber, respectively.

Selection of Standard Starting Conditions. As was shown in the previous section, it takes some finite time for an airfoil at angle of attack,  $\alpha$ , suddenly placed into motion to build to a steady-state value of lift. It is not surprising, then, to find that the onset of constant  $\dot{\alpha}$  demonstrates a different result depending on the time delay from onset of impulsive motion to onset of constant  $\dot{\alpha}$ . The differences, however, were found to be predictable, and thus separable, as the following will show.

To determine the effect the initial  $\alpha$  and  $\dot{\alpha}$  start time have on the  $C_l$  vs.  $\alpha$  curve for an airfoil at constant  $\dot{\alpha}$ , a 15% thick symmetric Joukowski airfoil with  $\dot{\alpha} = 0.01$ ,  $\Delta t^* = 0.02$  was started at various initial  $\alpha$ 's and allowed to build lift at that  $\alpha$  for varying lengths of time  $t^*$ . For initial  $\alpha = 0^\circ$ , one can see from Fig. 13 that the time  $t^*$

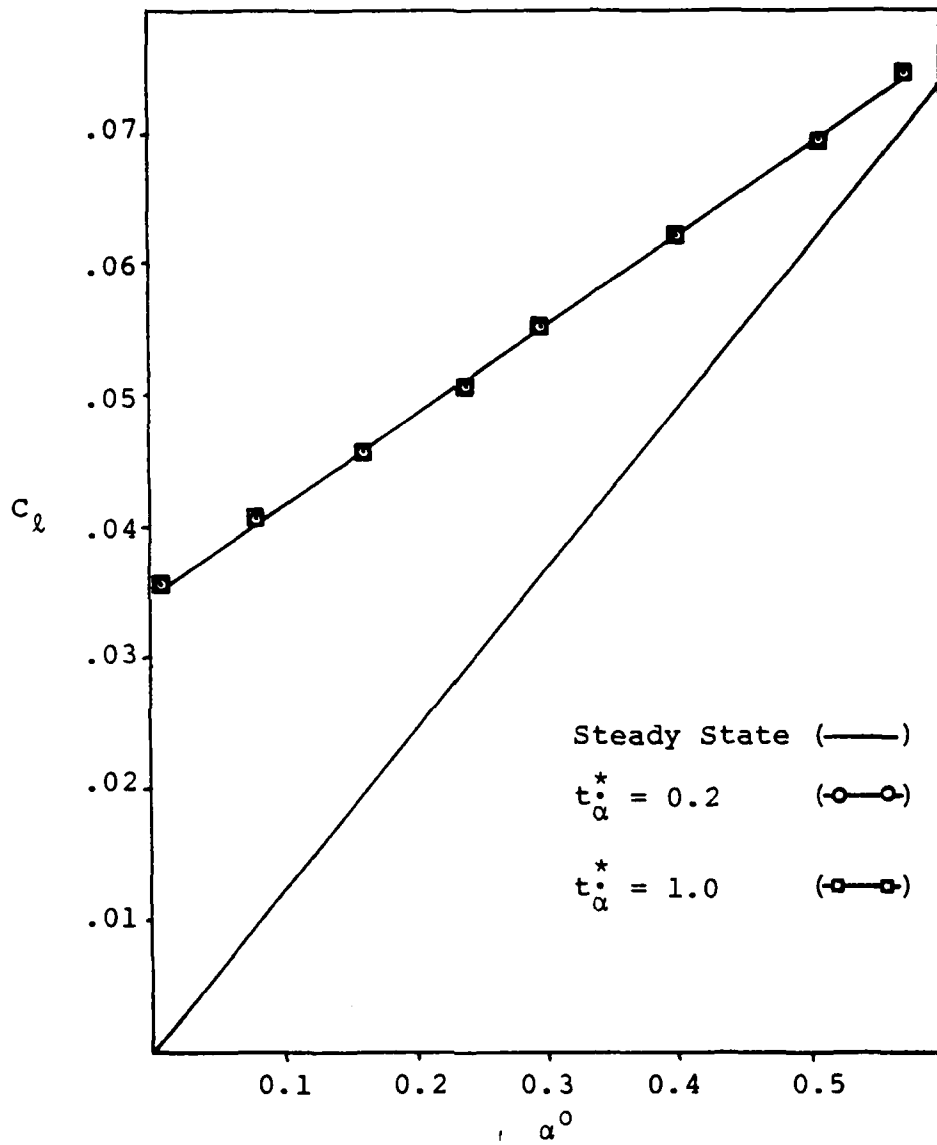


Fig. 13. Effect of Start Time to Begin  $\dot{\alpha}$   
 15% Joukowski Airfoil,  $\alpha_0 = 0^\circ$ ,  $\dot{\alpha}^* = 0.01$

at which the  $\dot{\alpha}$  begins has no effect on the  $C_\ell$  vs.  $\alpha$  curve. For initial  $\alpha = 5^\circ$ , the  $C_\ell$  vs.  $\alpha$  curves were dependent upon the value of  $t^*$  at which the  $\dot{\alpha}$  was begun. However, as can be seen in Fig. 14, the slope of the  $C_\ell$  vs.  $\alpha$  curve for  $\dot{\alpha} = 0.01$  does not depend upon the value of  $t^*$  at which the  $\dot{\alpha}$  was begun. Choosing  $\Delta t^* = 0.1$ , the 15% thick symmetric Joukowski airfoil was allowed to build lift to within 90% of steady-state  $C_\ell$  at various initial  $\alpha$ 's before starting an  $\dot{\alpha}^* = 0.01$ . As seen in Fig. 15, the slope of the  $C_\ell$  vs.  $\alpha$  curves for initial  $\alpha$ 's of  $2^\circ$ ,  $4^\circ$  and  $6^\circ$  are all approximately equal. The dashed lines on Fig. 15 depict the  $C_\ell$  vs.  $\alpha$  curves that would be obtained by starting the constant  $-\dot{\alpha}$  motion at full steady-state lift values rather than the 90% steady-state lift values depicted by the solid lines. Note that the initial value of  $C_\ell$  obtained for each of the starting angles of attack of  $2^\circ$ ,  $4^\circ$  and  $6^\circ$  is the same amount above the steady-state  $C_\ell$  curve, and is therefore independent of initial angle of attack. This initial value of  $C_\ell$  will be called the 'jump' condition. Thus, by the foregoing analysis,  $C_\ell$  vs.  $\alpha$  curve slope effects due to the vortex wake will be assumed independent of initial  $\alpha$  and  $t^*$ .

The choice of  $\Delta t^*$  also shows some effect on the  $C_\ell$  vs.  $\alpha$  curve and was investigated. To do this, a 15% thick symmetric Joukowski airfoil at  $\dot{\alpha}^* = 0.01$  was run at  $\Delta t^*$  values of 0.2, 0.1, 0.02 and 0.004. Figure 16 depicts a comparison of  $C_\ell$  vs.  $\alpha$  curves for these four values of  $\Delta t^*$ .



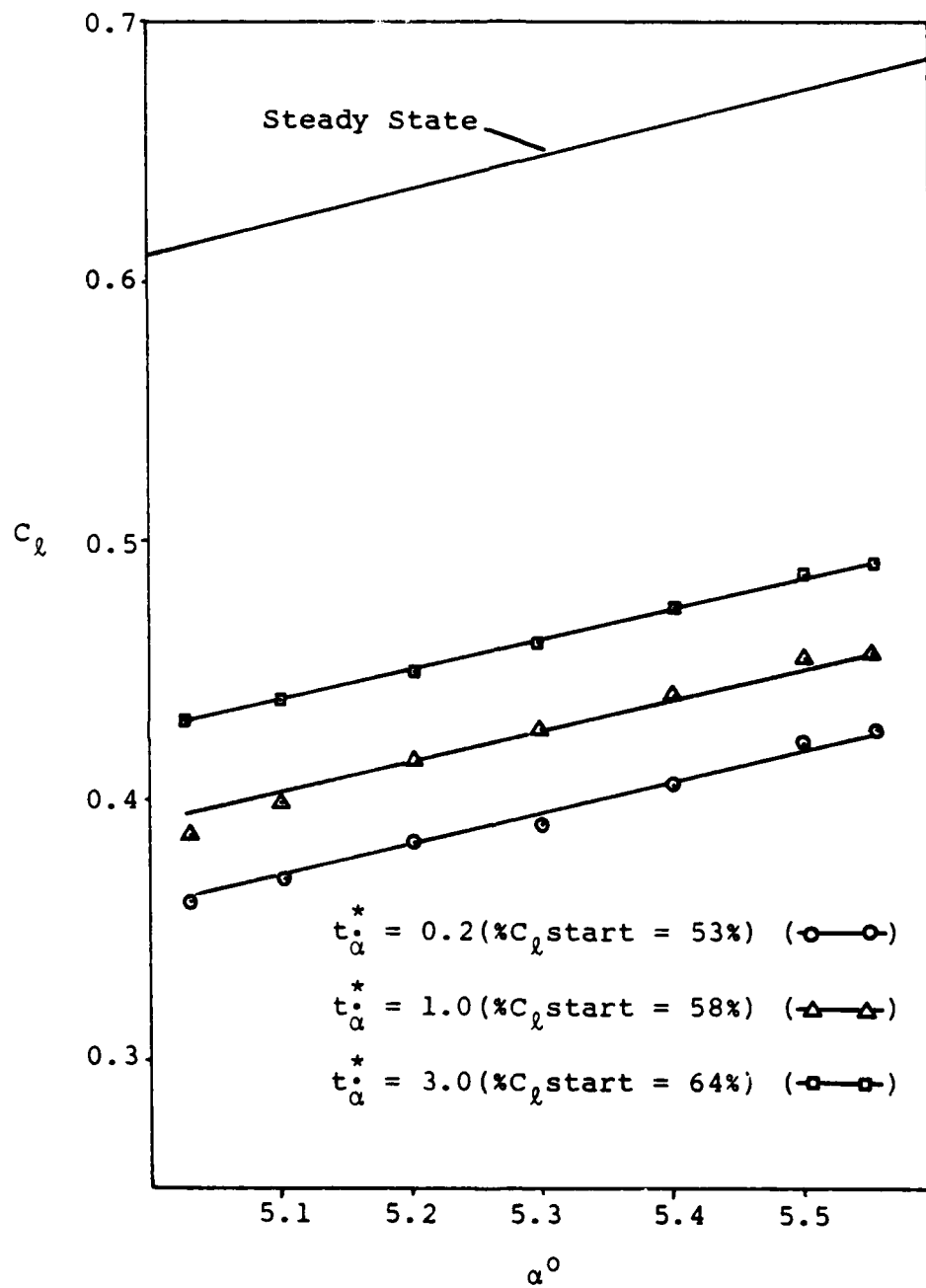


Fig. 14. Effect of Start Time to Begin  $\dot{\alpha}$   
 15% Joukowski Airfoil,  $\alpha_0 = 5^\circ$ ,  $\dot{\alpha}^* = 0.01$

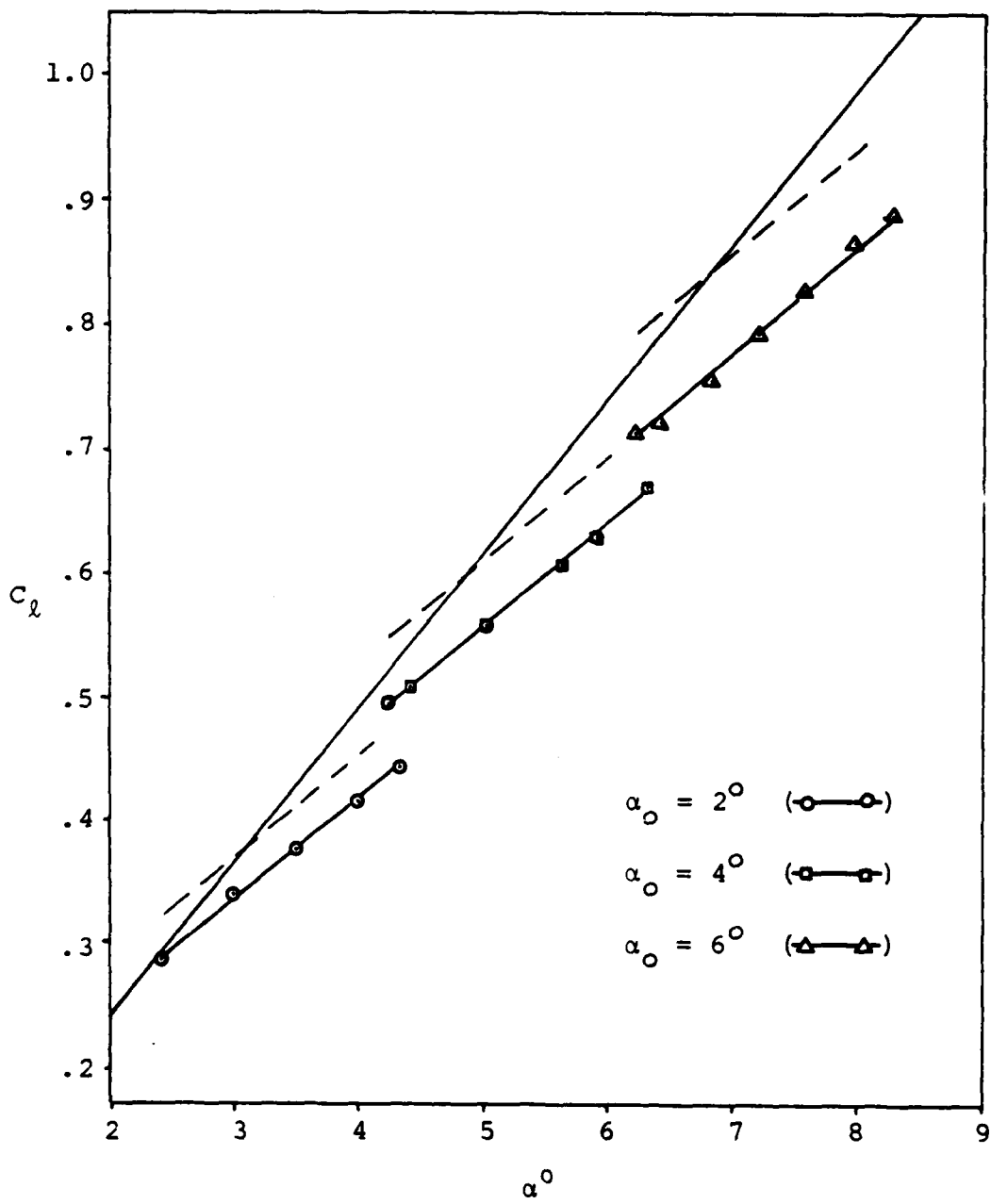


Fig. 15. Effect of Initial Angle of Attack to Begin  $\dot{\alpha}$  ( $C_l$  at 90% Steady-State Value)

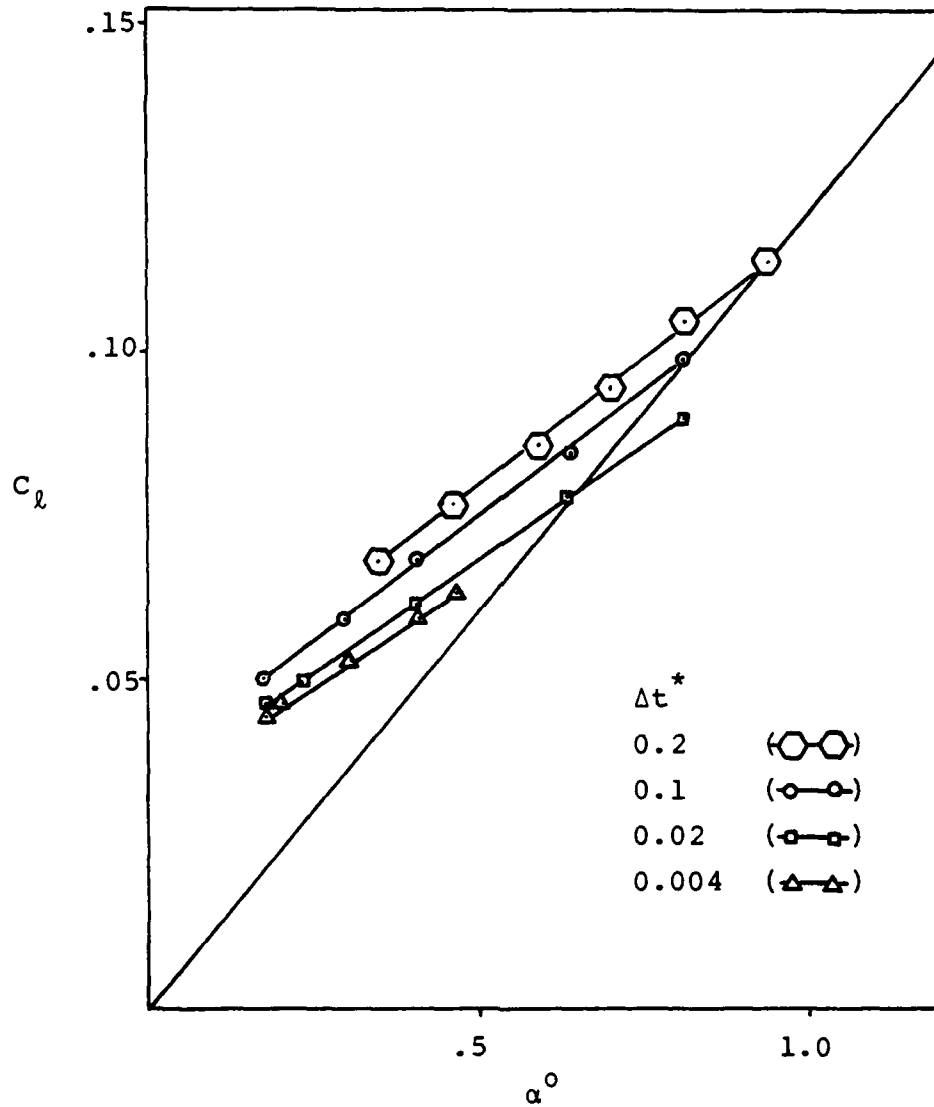


Fig. 16. Effect of  $\Delta t^*$  on  $C_l$  vs.  $\alpha$  Curve Slope  
 15% Joukowski Airfoil,  $\alpha_0 = 0^\circ$ ,  $\dot{\alpha}^* = 0.01$

Note that the slope of the curves,  $C_{l\alpha}$ , reduces as  $\Delta t^*$  is reduced, but the reduction is negligible below  $\Delta t^* = 0.02$ .

As a result of the above analysis concerning initial  $\alpha$  and  $t^*$  at which  $\dot{\alpha}$  is begun, all constant- $\dot{\alpha}$  computer runs assumed an initial  $\alpha = 0^\circ$  and  $t^* = 0$  for  $\dot{\alpha}$  start-up. A standard  $\Delta t^* = 0.02$  was chosen as a reasonable value based upon the information presented in Fig. 5 for impulsive-start motion and Fig. 16 for constant- $\dot{\alpha}$  motion. While a  $\Delta t^*$  less than 0.02 would produce more accurate results, the increased computer time required at the smaller  $\Delta t^*$  values was judged excessive for the slight increase in accuracy that could be obtained.

General Effect of  $\dot{\alpha}$  on  $C_{l\alpha}$ . To determine the effect an  $\dot{\alpha}$  has on the production of lift on an airfoil, a 15% thick symmetric Joukowski airfoil was chosen as a representative airfoil shape. Using the selected values of initial  $\alpha = 0^\circ$  and  $\Delta t^* = 0.02$ , the airfoil was subjected to various values of  $\dot{\alpha}^*$  ranging from 0.005 to 0.035. Figure 17 depicts the  $C_l$  vs.  $\alpha$  curves obtained for small angles of attack. Comparing with the  $C_l$  vs.  $\alpha$  curve for the steady-state case, one can see that as the value of  $\dot{\alpha}^*$  is increased, the slope of the  $C_l$  vs.  $\alpha$  curve,  $C_{l\alpha}$ , is reduced. As the motion progresses to larger values of  $\alpha$ , the slopes of the curves increase slightly (see Fig. 18).

Effect of Airfoil Thickness on  $\dot{\alpha}$  Effect. The general effect  $\dot{\alpha}$  has on the production of lift on an airfoil has been shown. This effect was shown for a specific airfoil only.

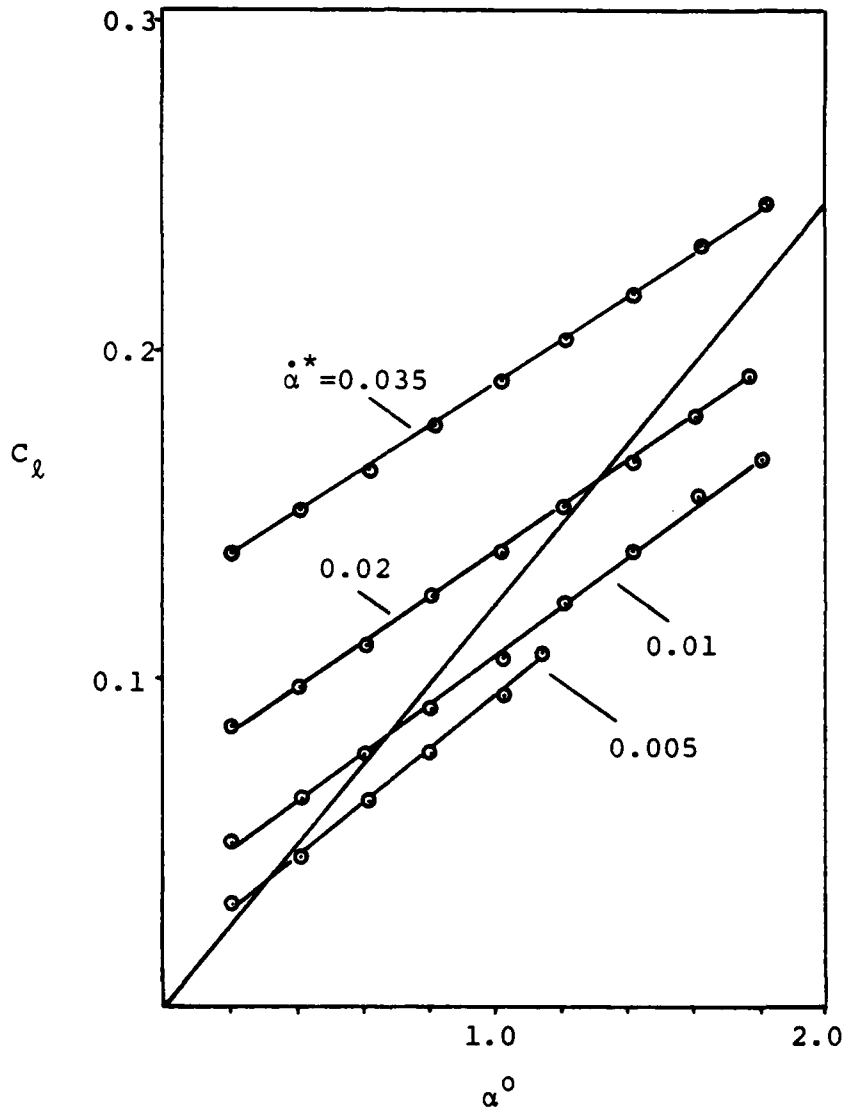


Fig. 17. Effects of  $\dot{\alpha}$  on  $C_l$  vs.  $\alpha$   
15% Joukowski Airfoil

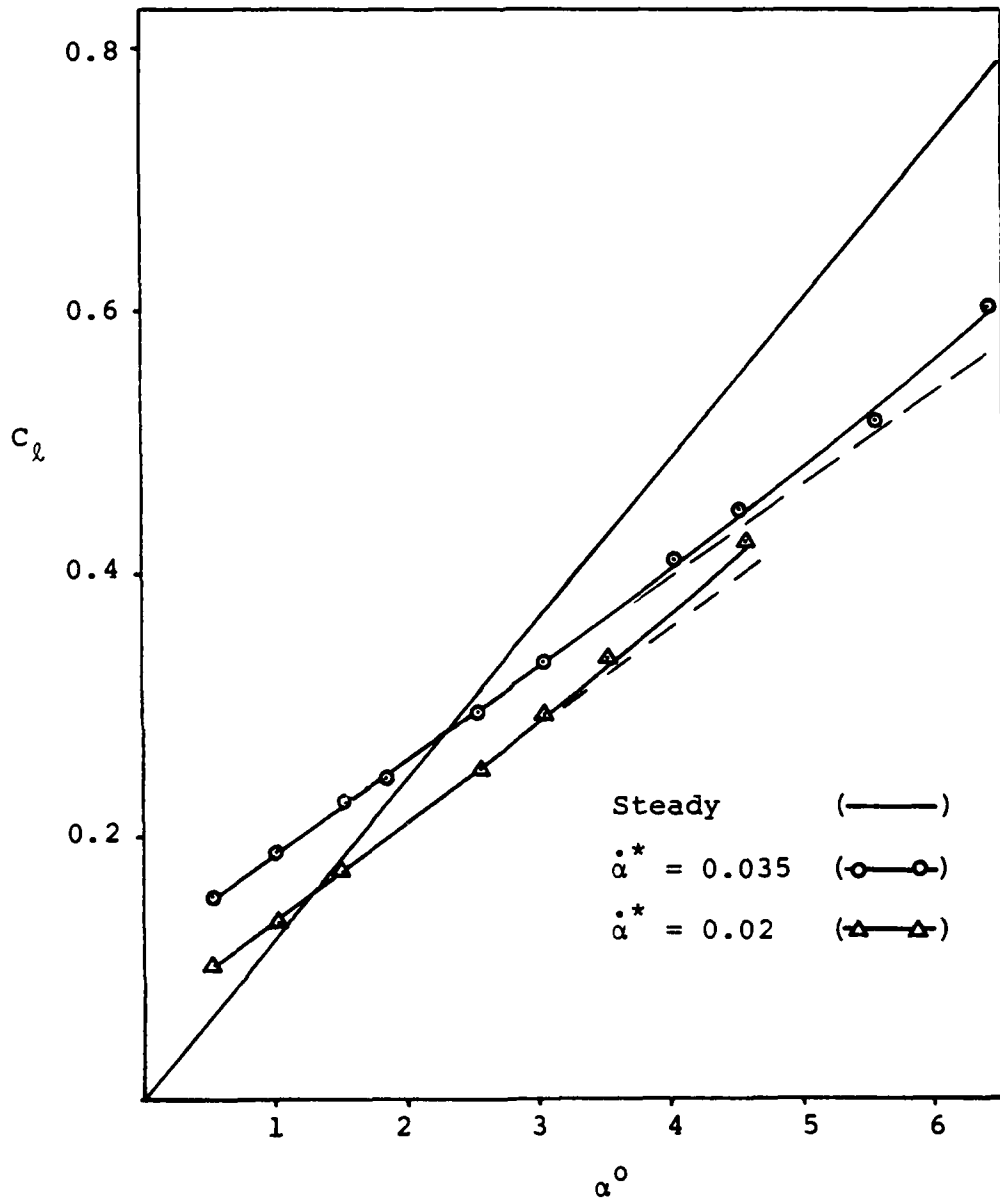


Fig. 18.  $C_l$  vs.  $\alpha$  Slope Change as  $\alpha$  Increases at Constant  $\dot{\alpha}$

To determine how airfoil thickness may influence this effect, several symmetric Joukowski airfoils of varying thickness were subjected to the same  $\dot{\alpha}$  conditions. Once again, values of  $\Delta t^* = 0.02$ , initial  $\alpha = 0^\circ$  were used. Symmetric Joukowski airfoils of 7%, 15% and 25.5% thickness, as well as a flat plate airfoil, were subjected to  $\dot{\alpha}^* = 0.02$ . A  $C_l$  vs.  $\alpha$  curve can be plotted for each of these airfoils. Plotting the average slopes of these curves,  $C_{l\alpha}$ , versus airfoil thickness ratio  $t/c$  (where  $t$  is the maximum airfoil thickness), one can determine the effect of airfoil thickness on the  $C_l$  vs.  $\alpha$  curve slope reduction due to  $\dot{\alpha}$ . Figure 19 depicts  $C_{l\alpha}$  vs.  $t/c$  for  $\dot{\alpha}^* = 0.02$ . One can see that  $\dot{\alpha}$  has a greater effect on lift curve slope reduction for thin airfoils than for thick airfoils. This effect is consistent with results previously presented. Note that in Fig. 9, where  $\dot{\alpha} = 0$ , for any given value of  $U_\infty \Delta t / \frac{1}{2}c$ , the slope of the  $C_l / C_{l_{ss}}$  curve is slightly greater for the 25.5% thick symmetric Joukowski airfoil than for the flat plate. Although the value of  $C_l / C_{l_{ss}}$  is less for the airfoil with thickness, the rate at which  $C_l / C_{l_{ss}}$  is increasing is greater. This implies that, under similar  $\dot{\alpha}$  conditions,  $C_l$  will increase at a faster rate for a thick airfoil than for a thin airfoil. Figure 19 confirms that conclusion.

Effect of Airfoil Camber on  $\dot{\alpha}$  Effect. In much the same way as airfoil thickness effects are calculated, airfoil camber effects can also be explored. Joukowski airfoils of 15% thickness at various camber ratios were subjected to an

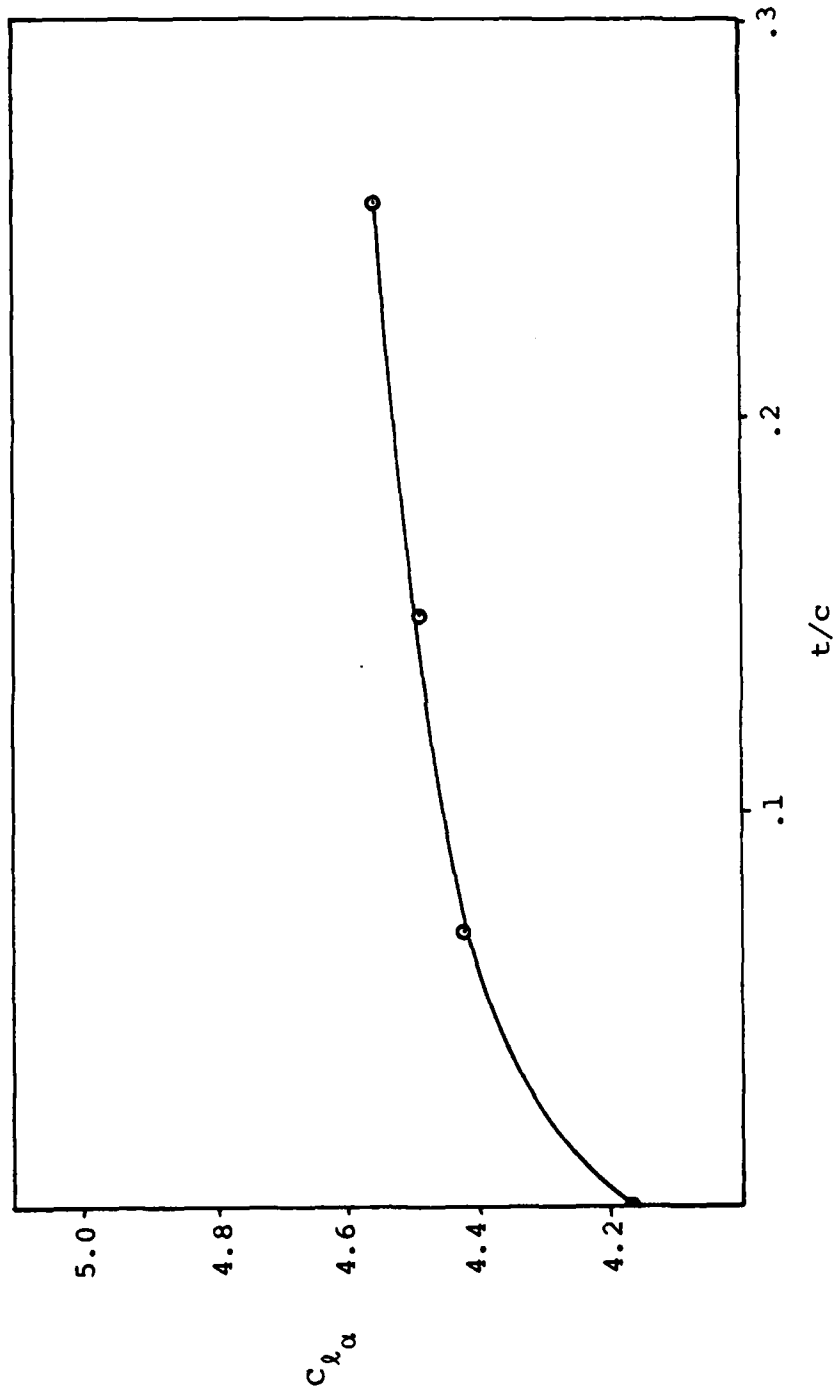


Fig. 19. Airfoil Thickness Effect on  $C_{l\alpha}$ ,  $\alpha^* = 0.02$



$\dot{\alpha}^* = 0.02$  . As before, initial  $\alpha$  was  $0^\circ$ ,  $\Delta t^* = 0.02$  .  
Plotting average  $C_{l\alpha}$  versus camber ratio (maximum camber/  
chord), camber effects can be shown. Figure 20 depicts  $C_{l\alpha}$   
vs. camber ratio for 15% thick Joukowski airfoils of various  
camber ratios. One can see that  $\dot{\alpha}$  has a greater effect on  
lift curve slope reduction for less cambered airfoils than  
for highly cambered airfoils.

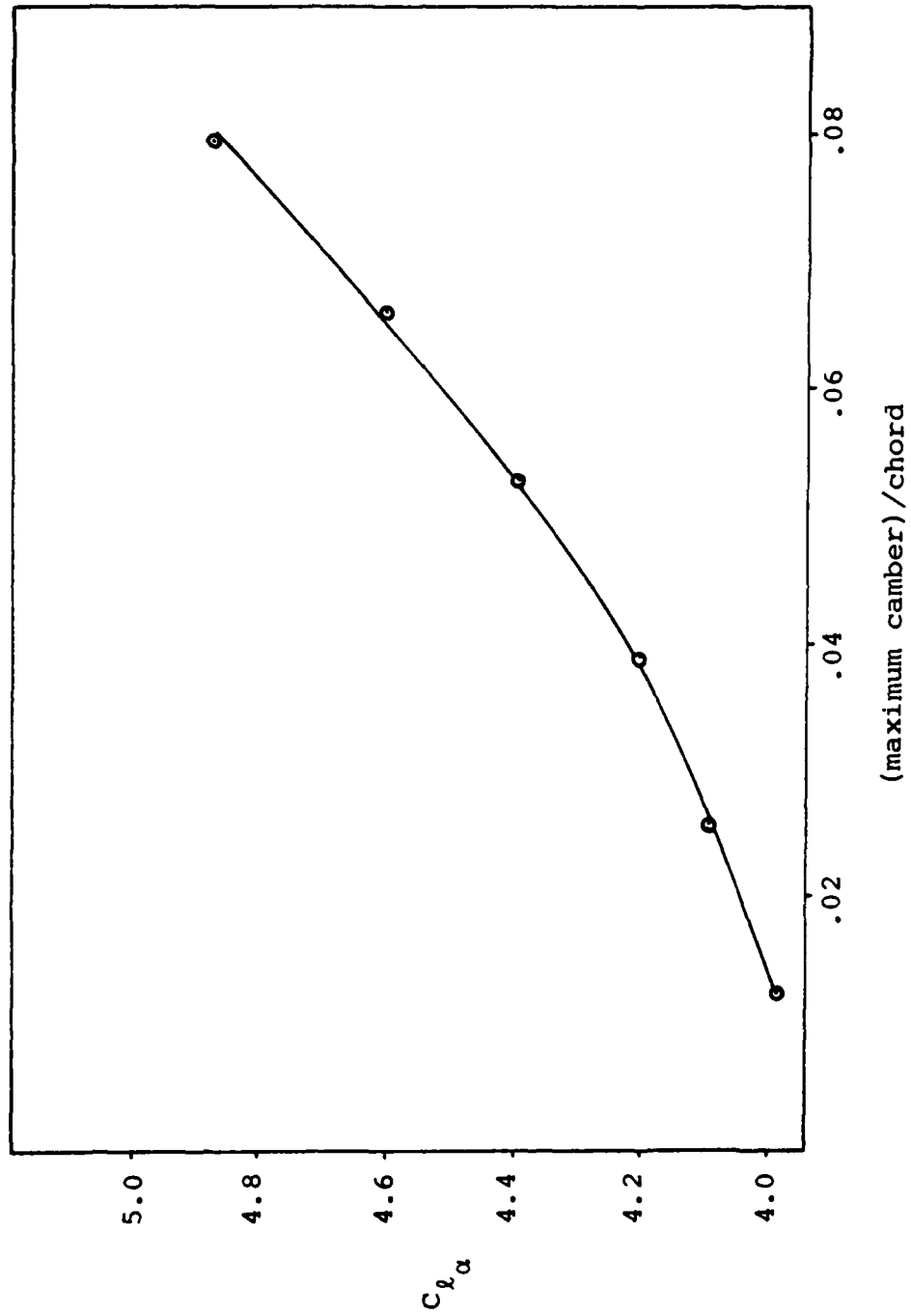


Fig. 20. Airfoil Camber Effect on  $C_{l_{\alpha}}$ ,  $\alpha^* = 0.02$

#### IV. Conclusion

It has been shown that as an airfoil pitches at a constant  $\dot{\alpha}$ , the airfoil trailing vortex wake causes the slope of the  $C_{l\alpha}$  vs.  $\alpha$  curve to be less than the slope of the  $C_l$  vs.  $\alpha$  curve for steady-state  $\alpha$ . The greater the value of  $\dot{\alpha}$  for a given airfoil, the greater the slope reduction of the  $C_l$  vs.  $\alpha$  curve caused by the vortex wake. This effect becomes less pronounced as airfoil thickness increases. Similarly, the effect is also less pronounced as airfoil camber increases.

Using the results from the previous section, the following predictions of constant- $\dot{\alpha}$  effect may be made.

For a flat plate, the reduction in  $C_{l\alpha}$  may be approximately calculated by

$$C_{l\alpha}(\dot{\alpha}^*) = \frac{1}{(\dot{\alpha}^* + 0.00008)^{0.15}} + 2.2 \quad (49)$$

(See Fig. 21 for a comparison of this prediction with numerical data.) This prediction may be approximately corrected for thickness by adding a correction term derived from Fig. 19. Thus

$$C_{l\alpha}(\dot{\alpha}^*, t/c) = \left(\frac{t}{c}\right)^{0.75} + C_{l\alpha}(\dot{\alpha}^*) \quad (50)$$

where  $t/c$  is the airfoil thickness to chord ratio and  $C_{l\alpha}(\dot{\alpha}^*)$  is the  $C_l$  vs.  $\alpha$  curve slope for a flat plate predicted by Eq. (49). A further approximate correction may be made for camber by adding another correction term, derived from Fig. 20. Thus

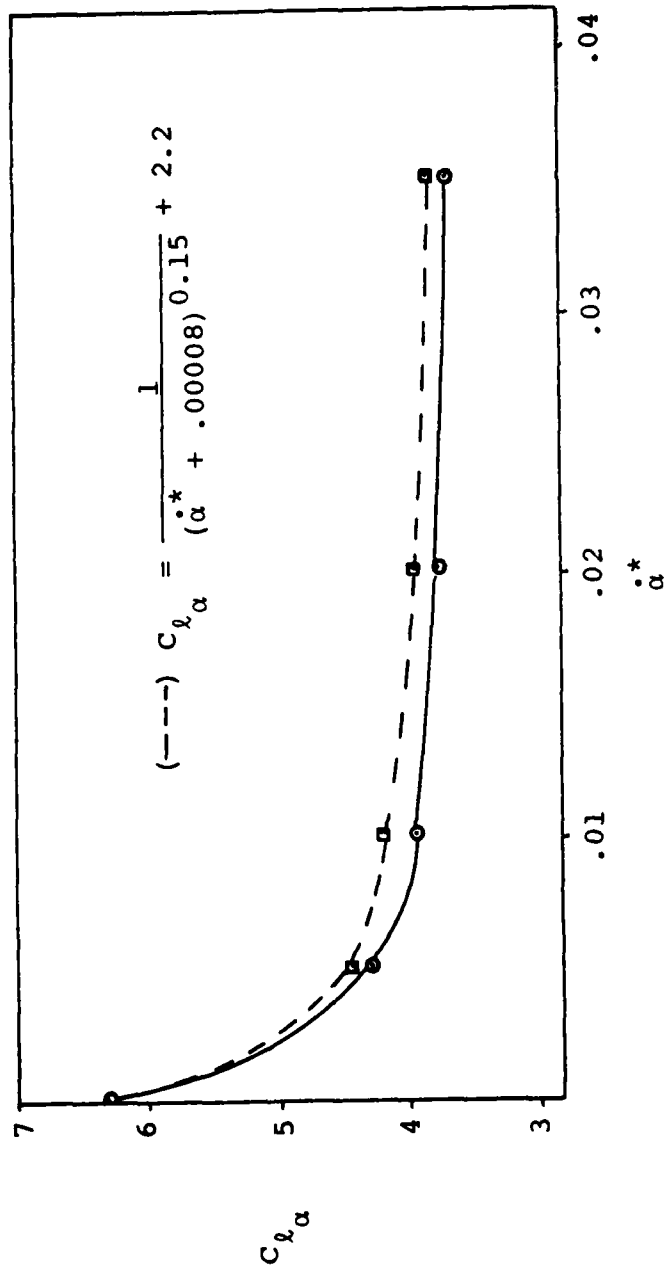


Fig. 21. Flat Plate  $C_{l\alpha}$  Changes as a Function of  $\dot{\alpha}$

$$C_{\ell\alpha}(\dot{\alpha}^*, t/c, mc/c) = e^{30(mc/c-0.09)} + C_{\ell\alpha}(\dot{\alpha}^*, t/c) \quad (51)$$

where  $mc/c$  is the airfoil camber ratio and  $C_{\ell\alpha}(\dot{\alpha}^*, t/c)$  is the  $C_\ell$  vs.  $\alpha$  curve slope for an airfoil with thickness predicted by Eq. (50).

The amount that  $C_\ell$  increases immediately after an airfoil begins constant- $\dot{\alpha}$  motion is referred to as the 'jump' condition. This value for a flat plate can be predicted by

$$\Delta C_\ell(\dot{\alpha}^*) = 3.47\dot{\alpha}^* \quad (52)$$

where  $\Delta C_\ell(\dot{\alpha}^*)$  is the 'jump' condition change. Thickness effects on  $\Delta C_\ell(\dot{\alpha}^*)$  can be approximated by the equation

$$\Delta C_\ell(\dot{\alpha}^*, t/c) = \left[1 + \frac{2(t/c)}{3}\right] \Delta C_\ell(\dot{\alpha}^*) \quad (53)$$

where  $t/c$  is the airfoil thickness ratio and  $\Delta C_\ell(\dot{\alpha}^*)$  is the 'jump' condition for a flat plate defined by Eq. (52). A final approximate correction to the 'jump' condition can be made by

$$\Delta C_\ell(\dot{\alpha}^*, t/c, mc/c) = \Delta C_\ell(\dot{\alpha}^*, t/c) - 1.3\left(\frac{mc}{c}\right) \quad (54)$$

where  $mc/c$  is the airfoil camber ratio and  $\Delta C_\ell(\dot{\alpha}^*, t/c)$  is as defined by Eq. (53).

## V. Recommendation

The assumption that the trailing vortex wake of an airfoil undergoing a constant rate of change of angle of attack has a negligible effect on the production of lift on the airfoil is not, in general, valid. Although the effect is not large (see Eq. (49)), it should be accounted for in the investigation of dynamic stall of airfoils. The methods developed by Docken (4) and Lawrence (5) could be modified to include the techniques presented in this thesis to more accurately predict the potential flow field about a pitching airfoil at any instant in time. Incorporating the calculation of wake vortex effects outlined in this thesis into Lawrence's work would significantly contribute to the solution of the dynamic stall problem for an airfoil undergoing a constant rate of change of angle of attack.

## APPENDIX: Computer Program

```

C
C   This program computes circulation, pressure difference
C   distribution, vorticity distribution, coefficient of
C   lift, and trailing vortex wake shape for a 2-D Joukowski
C   airfoil in an incompressible, inviscid free stream at
C   angle of attack. The angle of attack may be a constant
C   value, or it may be changed at a constant rate for the
C   number of time steps desired. All output values are
C   computed assuming a trailing vortex wake made up of dis-
C   crete point vortices of constant strength, each of which
C   influences the motion of all the other vortices and the
C   flow about the airfoil. For the constant rate-of-change
C   of angle-of-attack case, coefficient of lift can be
C   found as a function of the rate of change of angle of
C   attack. Variables in the program are defined as follows:
C
C   alfa          - angle of attack
C   alfa0         - initial angle of attack
C   alfdot        - time rate of change of angle of attack
C   beta          - the beta parameter of a Joukowski airfoil
C   calfa         - COSINE of alfa
C   chord         - airfoil chord length
C   cl            - coefficient of lift
C   clss          - steady-state coefficient of lift
C   countt       - an integer counter used to determine which
C                 time steps will record output in certain
C                 files
C   ctheta        - COSINE of theta
C   dalfa         - incremental change of alfa
C   delcp         - array of incremental values of coefficient
C                 of pressure along the airfoil chord
C   deld          - distance on the x-axis in the cylinder
C                 plane behind the cylinder where the first
C                 shed vortex is placed
C   delgam        - array of values of strengths of gamma for
C                 each individual vortex pair
C   dgams         - a sum of vortex strengths
C   dsl           - incremental distance along airfoil lower
C                 surface
C   dsu           - incremental distance along airfoil upper
C                 surface
C   dt            - incremental unit of time
C   DZD           - complex number; derivative of the
C                 Joukowski transformation
C   dzdrc        - magnitude of DZD
C   eta          - x-value of trailing vortex position

```

|   |             |   |
|---|-------------|---|
| C | eta2        | - x-value of trailing vortex image position   |
| C | gamma       | - airfoil circulation   |
| C | i,j,k,l     | - integer values used in iterations   |
| C | intgr1      | - value of the integration of velocity differences between upper and lower airfoil surfaces                                     |
| C | lastdt      | - last time increment at which alfa changes   |
| C | mag2        | - distance from a vortex to the center of the cylinder in the cylinder-centered plane   |
| C | malfa       | - maximum value of alfa   |
| C | maxdt       | - first time increment at which alfa changes from alfa0   |
| C | maxt        | - last time step  |
| C | MU          | - complex number; distance between the origin in the displaced-cylinder plane and the center of the cylinder                    |
| C | pi          | - the constant 3.14159265   |
| C | RHO         | - complex number; a position in the cylinder-centered plane   |
| C | RHOP        | - complex number; a position in the displaced-cylinder plane  |
| C | salfa       | - SINE of alfa  |
| C | ssgam       | - steady state value of circulation   |
| C | stheta      | - SINE of theta   |
| C | sumsq       | - the square of the distance of a trailing vortex from the origin in the cylinder plane   |
| C | sumu,sumv   | - sum of the velocities on the cylinder in the x and y directions, respectively, induced by trailing vortices and their images  |
| C | t           | - integer counter for number of time steps  |
| C | theta       | - angle measured counterclockwise from the x-axis in the cylinder plane   |
| C | totu,totv   | - sum of velocities at a vortex location in the x and y directions, respectively, induced by trailing vortices and their images |
| C | u,v         | - velocities at a vortex location in the x and y directions, respectively   |
| C | ua,va       | - velocities at a vortex location in the x and y directions, respectively, in the airfoil plane                                 |
| C | usurf,vsurf | - velocities on the cylinder in the x and y directions, respectively  |
| C | utheta      | - velocity tangent to the cylinder  |
| C | vordis      | - vorticity   |
| C | vsqare      | - velocity on upper surface of airfoil squared minus velocity on lower surface of airfoil squared                               |
| C | x,y         | - position on airfoil   |
| C | xvort,yvort | - position of a trailing vortex   |
| C | Z           | - complex number; a position on the airfoil   |
| C | zeta        | - y value of trailing vortex position   |
| C | zeta2       | - y value of trailing vortex image position   |



```

C   zt          - distance along x-axis from origin to
C               cylinder in displaced-cylinder plane
C   ZZ          - complex number; a position in the wake in
C               the airfoil plane

```

```

C           FILES:

```

```

C   INPUT      - unformatted list of input variables
C   OUTPUT     - list of Cl vs. Cl steady-state for angle of
C               attack and time step
C   PRESD      - pressure distribution at specified time
C   VORT       - vorticity distribution at specified time
C   WAKE       - position of trailing vortices at specified time
C

```

```

      DIMENSION zeta(201,201),eta(201,201),eta2(201,201),
+             zeta2(201,201),u(201,201),v(201,201),delgam(201),
+             x(-180:180),y(-180:180),utheta(-180:180),uo(201,201),
+             va(201,201),xvort(201,201),yvort(201,201),
+             vordis(0:176),delcp(0:176),intgr1(0:201,0:180)
      INTEGER i,j,maxt,t,k,l,maxdt,countt
      REAL delgam,deld,pi,ctheta,stheta,ssgam,dsu,dsl,delcp,
+         usurf,vsurf,theta,utheta,gamma,malfa,alfa,sumu,sumv,
+         dalfa,dgams,calfa,salfa,sumsq,alfdot,dt,dzdro,ua,va,
+         beta,zt,alfa0,clss,cl,x,y,vsqare,xvort,yvort,lastdt,
+         eta2,zeta,zeta2,u,v,chord,intgr1,totu,totv,vordis,
+         tmag2,eta
      COMPLEX MU,RHOP,Z,ZZ,RHO,DZD
      OPEN (15,FILE='INPUT')
      REWIND 15
      OPEN (16,FILE='OUTPUT')
      REWIND 16
      OPEN (17,FILE='PRESD')
      REWIND 17
      OPEN (18,FILE='WAKE')
      REWIND 18
      OPEN (19,FILE='VORT')
      REWIND 19
      pi=3.14159265

```

```

C   Initialize delta alpha, delta d, max t. Compute steady
C   state gamma.
C

```

```

10 CONTINUE
      READ(15,*,END=400) beta,alfa0,dalfa,deld,maxdt,maxt,
+         lastdt,zt,alfdot,dt
      malfa=dalfa*(lastdt-maxdt)+alfa0
      ssgam=4*pi*SIN(malfa*pi/180)
      WRITE(16,70) zt,beta,dalfa,deld,ssgam,alfdot,dt
      WRITE(17,72) zt,beta,dalfa,deld,ssgam,alfdot,dt

```

```

WRITE(18,72) zt,beta,dalfa,deld,ssgam,alldot,dt
WRITE(19,72) zt,beta,dalfa,deld,ssgam,alldot,dt
beta=beta*pi/180
dalfa=dalfa*pi/180
alfa0=alfa0*pi/180
MU=CMPLX(zt-COS(beta),SIN(beta))

```

C  
C  
C

Calculate coordinates of points on the airfoil. (x,y)

```

DO 15 i=-180,180
  theta=i*pi/180
  RHOP=CMPLX(COS(theta-beta),SIN(theta-beta))+MU
  Z=RHOP+zt**2/RHOP
  x(i)=REAL(Z)
  y(i)=AIMAG(Z)
15 CONTINUE
  chord=x(0)-x(-180+2*beta)
  DO 12 i=1,maxt
    delgam(i)=0.0
12 CONTINUE
  DO 13 i=176,0,-4
    intgr1(0,i)=0.
13 CONTINUE

```

C  
C  
C  
C

Begin stepping in time, inserting a new vortex pair at each time step.

```

countt=0
DO 300 t=1,maxt
  countt=countt+1
  intgr1(t,180)=0.
  dgams=0.0
  cl=0.
  IF (t.GE.maxdt.and.t.LE.lastdt) THEN
    alfa=(t-maxdt)*dalfa+alfa0
  ELSE IF (t.LT.maxdt) THEN
    alfa=alfa0
  END IF
  calfa=COS(alfa)
  salfa=SIN(alfa)

```

C  
C  
C  
C

Insert new vortex pair, and update position of all other vortex images.

```

  zeta(t,1)=deld+1.
  eta(t,1)=0.
  xvort(t,1)=chord*dt*COS(2*beta)/2+x(0)
  yvort(t,1)=chord*dt*SIN(2*beta)/(-2)
  DO 20 j=1,t
    zeta2(t,j)=zeta(t,j)/(zeta(t,j)**2+eta(t,j)**2)
    eta2(t,j)=eta(t,j)/(zeta(t,j)**2+eta(t,j)**2)
20 CONTINUE

```

```

C
C Calculate strength of newly shed vortex at time t.
C This is done by satisfying the Kutta Condition at the
C trailing edge while keeping total circulation in the
C field equal to zero.
C
delgam(1)=4*pi*salfa*(zeta(t,1)**2+eta(t,1)**2+1-2*
+ zeta(t,1))/(zeta(t,1)**2+eta(t,1)**2-1)
IF(t.GE.2) THEN
  DO 21 i=t,2,-1
    dgams=dgams+delgam(i)*(zeta(t,i)**2+eta(t,i)**2-1)
+ /((zeta(t,i)**2+eta(t,i)**2+1-2*zeta(t,i))*
+ delgam(1)/(4*pi*salfa)
21 CONTINUE
END IF
delgam(1)=delgam(1)-dgams
C
C Compute velocities and circulation around the cylinder
C at time t.
C
DO 200 i=-178,178,2
  theta=i*pi/180
  ctheta=COS(theta)
  stheta=SIN(theta)
  sumu=0.0
  sumv=0.0
  DO 30 k=t,1,-1
    sumu=delgam(k)/2/pi*((eta(t,k)-stheta)/((ctheta-
+ zeta(t,k))**2+(stheta-eta(t,k))**2)+(stheta-
+ eta2(t,k))/((ctheta-zeta2(t,k))**2+(stheta-
+ eta2(t,k))**2))+sumu
    sumv=delgam(k)/2/pi*((ctheta-zeta(t,k))/((ctheta-
+ zeta(t,k))**2+(stheta-eta(t,k))**2)-((ctheta-
+ zeta2(t,k))/((ctheta-zeta2(t,k))**2+(stheta-
+ eta2(t,k))**2))+sumv
30 CONTINUE
  usurf=2*(calfa*stheta**2-ctheta*stheta*salfa)+sumu
  vsurf=2*(salfa*ctheta**2-ctheta*stheta*calfa)+sumv
  utheta(i)=SQRT(usurf**2+vsurf**2)
  IF(i.NE.0) THEN
    RHOP=CMPLX(COS(theta-beta),SIN(theta-beta))+MU
    DZD=1-zt**2/RHOP**2
    dzdro=ABS(DZD)
    utheta(i)=utheta(i)/dzdro
  END IF
  IF((theta-(alfa+2*beta)).LT.-1*pi) THEN
    utheta(i)=-1*utheta(i)
  END IF
200 CONTINUE
  gamma=0.
  DO 210 i=1,t
    gamma=gamma+delgam(i)

```

210 CONTINUE

```
C
C   Compute velocity at each discrete vortex location due
C   to all other vortices and free stream.
C
      DO 50 l=1,t
        totu=0.0
        totv=0.0
        DO 40 k=1,t
          IF(k.EQ.1) THEN
            totu=delgam(k)/2/pi*((eta(t,k)-eta2(t,k))/((
+             zeta(t,k)-zeta2(t,k))**2+(eta(t,k)-eta2(t,k))
+             **2))+totu
            totv=delgam(k)/2/pi*((zeta2(t,k)-zeta(t,k))/((
+             zeta(t,k)-zeta2(t,k))**2+(eta(t,k)-eta2(t,k))
+             **2))+totv
          ELSE
            totu=delgam(k)/2/pi*((eta(t,l)-eta2(t,k))/((
+             zeta(t,l)-zeta2(t,k))**2+(eta(t,l)-eta2(t,k))
+             **2)+(eta(t,k)-eta(t,l))/((zeta(t,l)-zeta(t,k))
+             **2+(eta(t,l)-eta(t,k))**2))+totu
            totv=delgam(k)/2/pi*((zeta2(t,k)-zeta(t,l))/((
+             zeta(t,l)-zeta2(t,k))**2+(eta(t,l)-eta2(t,k))
+             **2)+(zeta(t,l)-zeta(t,k))/((zeta(t,l)-zeta(t,k))
+             **2+(eta(t,l)-eta(t,k))**2))+totv
          END IF
        40 CONTINUE
        sumsqr=zeta(t,l)**2+eta(t,l)**2
        u(t,l)=calfa*(1+(eta(t,l)**2-zeta(t,l)**2)/sumsqr
+         **2)-2*zeta(t,l)*eta(t,l)*salfa/sumsqr**2+totu
        v(t,l)=salfa*(1+(zeta(t,l)**2-eta(t,l)**2)/sumsqr
+         **2)-2*zeta(t,l)*eta(t,l)*calfa/sumsqr**2+totv
      50 CONTINUE
C
C   Calculate pressure distribution and unsteady aerodynamic
C   force on the airfoil.
C
      DO 32 i=176,0,-4
        theta =i*pi/180
        ctheta=COS(theta)
        stheta=SIN(theta)
        dsu=SQRT((x(i)-x(i+4))**2+(y(i)-y(i+4))**2)*2/chord
        dsl=SQRT((x(-1*i)-x(-1*(i+4)))**2+(y(-1*i)-y(-1*
+         (i+4)))**2)*2/chord
        intgr1(t,i)=utheta(i+2)*dsu-utheta(-1*(i+2))*dsl
+         +intgr1(t,i+4)
        vsqare=utheta(i)**2-utheta(-1*i)**2
        IF(t.EQ.1) THEN
          delcp(i)=vsqare+2*intgr1(1,i)/dt
```

```

ELSE IF(t.EQ.2) THEN
  delcp(i)=vsqare+2*(intgr1(2,i)-intgr1(1,i))/dt
ELSE IF(t.EQ.maxdt) THEN
  delcp(i)=vsqare+2*intgr1(maxdt,i)/dt
ELSE IF(t.EQ.maxdt+1) THEN
  delcp(i)=vsqare+2*(intgr1(maxdt+1,i)-
    intgr1(maxdt,i))/dt
ELSE
  delcp(i)=vsqare+(intgr1(t-2,i)+3*intgr1(t,i)-4*
+   intgr1(t-1,i))/dt
END IF
IF(i.EQ.176) THEN
  cl=cl+delcp(176)*(x(174)-x(180))/chord
ELSE IF(i.EQ.0) THEN
  cl=cl+delcp(0)*(x(0)-x(2))/chord
ELSE
  cl=cl+delcp(i)*(x(i-2)-x(i+2))/chord
END IF
32 CONTINUE
C
C   Calculote Cl.
C
  class=8*pi/chord*salfa
  IF(t.EQ.3) THEN
    WRITE(17,('Delta Cp, ',I3,' Vortices, t=',F7.4)')
+   t,t*dt
    WRITE(19,('Vorticity Distribution ',I3,
+   ' Vortices, t=',F7.4)') t,t*dt
    DO 34 i=176,0,-4
      vordis(i)=utheta(i)-utheta(-1*i)
      WRITE(19,90) (x(i)+chord-2*zt)*2/chord,vordis(i)
      WRITE(17,90) (x(i)+chord-2*zt)*2/chord,-1*delcp(i)
34 CONTINUE
    END IF
    IF(countt/10.GT.0) THEN
      WRITE(17,('Delta Cp, ',I3,' Vortices, t=',F7.4)')
+   t,t*dt
      WRITE(19,('Vorticity Distribution ',I3,
+   ' Vortices, t=',F7.4)') t,t*dt
      DO 35 i=176,0,-4
        vordis(i)=utheta(i)-utheta(-1*i)
        WRITE(19,90) (x(i)+chord-2*zt)*2/chord,vordis(i)
        WRITE(17,90) (x(i)+chord-2*zt)*2/chord,-1*delcp(i)
35 CONTINUE
        countt=0
      END IF
      WRITE(16,80) t,(alfa-beta)*180/pi,(xvort(t,t)-x(0))
+   *2/chord,yvort(t,t)*2/chord,gamma,class,cl
C
C   Move each vortex to its new location in the flow field.
C

```

```

DO 60 K=t,1,-1
  mag2=SQRT(zeta(t,k)**2+eta(t,k)**2)
  RHOP=mag2*CMPLX(COS(ACOS(zeta(t,k)/mag2)-beta),
+   SIN(ASIN(eta(t,k)/mag2)-beta))+MU
  DZD=1-zt**2/RHOP**2
  dzdro=ABS(DZD)
  ua(t,k)=u(t,k)/dzdro
  va(t,k)=v(t,k)/dzdro
  xvort(t+1,k+1)=xvort(t,k)+ua(t,k)*chord*dt/2
  yvort(t+1,k+1)=yvort(t,k)+va(t,k)*chord*dt/2
  ZZ=CMPLX(xvort(t+1,k+1),yvort(t+1,k+1))
  RHO=((ZZ+ SQRT(ZZ**2-4*zt**2))/2-MU)*
+   CMPLX(COS(beta),SIN(beta))
  zeta(t+1,k+1)=REAL(RHO)
  eta(t+1,k+1)=AIMAG(RHO)
  delgam(k+1)=delgam(k)
60 CONTINUE
  IF(t.EQ.5) THEN
    GO TO 61
  ELSE IF (t.EQ.maxdt) THEN
    GO TO 61
  ELSE IF(t.EQ.lastdt) THEN
    GO TO 61
  ELSE IF(t.EQ.maxt) THEN
    GO TO 61
  ELSE
    GO TO 300
  END IF
61 WRITE(18,('Wake Vortex Locations from Trailing',
+ ' Edge (1/2 c = 1)')/' Xvort',5X,'Yvort')
  DO 65 i=1,t
    WRITE(18,95) (xvort(t,i)-x(0))*2/chord,
+   yvort(t,i)*2/chord
65 CONTINUE
300 CONTINUE
70 FORMAT(///,'AIRFOIL DATA :',//,'Zeta trailing edge :',
+ F7.4,' Beta (degrees):',F6.3,///,'DYNAMIC PARAMETERS',
+ //,'Delta Alpha (degrees):',F6.3,' Delta Vortex ',
+ 'Distance:',F6.4,/, 'Steady State Gamma: ',F7.5,
+ ' Alpha Dot:',F8.5,' Delta Time:',F5.3,///,'Time',10X,
+ 'Starting Vortex',17X,'Cl',/, 'Step Alpha X ',
+ ' Y Gamma Steady State Cl',/)
72 FORMAT(///,'AIRFOIL DATA :',//,'Zeta trailing edge :',
+ F7.4,' Beta (degrees):',F6.3,///,'DYNAMIC PARAMETERS',
+ //,'Delta Alpha (degrees):',F6.3,' Delta Vortex ',
+ 'Distance:',F6.4,/, 'Steady State Gamma: ',F7.5,
+ ' Alpha Dot:',F8.5,' Delta Time:',F5.3,/)
80 FORMAT(I3,3X,F6.3,2X,F7.4,F8.4,1X,F8.5,5X,F8.5,2X,F8.5)
90 FORMAT(F8.3,4X,F10.5)
95 FORMAT(F8.4,F11.4)
100 END

```

## Bibliography

1. Kramer, von M. "Die Zunahme des Maximalauftriebes von Tragflugeln bei plotzlicher AnstellwinkervergroBerung (Boeneffekt)," Zeitschrift fur Flugtechnik und Motorluftschiffahrt, 7: 185-189 (April 1932).
2. Deekens, A.C. and W.R. Kuebler, Jr. "A Smoke Tunnel Investigation of Dynamic Separation," Aeronautics Digest, Fall 1978. USAFA-TR-79-1, Air Force Academy, CO. Feb 1979.
3. Daley, D.C. The Experimental Investigation of Dynamic Stall. Thesis, AFIT/GAE/AA/82D-6. Air Force Institute of Technology, Wright-Patterson AFB, OH, 1983.
4. Docken, R.G., Jr. Gust Response Prediction of an Airfoil using a Modified vonKarman-Pohlhausen Technique. Thesis, AFIT/GAE/AA/82D-9, Air Force Institute of Technology, Wright-Patterson AFB, OH, 1982.
5. Lawrence, Maj J.S. Investigation of Effects Contributing to Dynamic Stall Using a Momentum-Integral Method. Thesis, AFIT/GAE/AA/83D-12. Air Force Institute of Technology, Wright-Patterson AFB, OH, 1983.
6. Shung, Yeou-Kuang. Numerical Solution for Some Problems Concerning Unsteady Motion of Airfoils. Ph.D. dissertation. University of Colorado, Boulder, CO, 1977.
7. Spiegel, Murray R. Theory and Problems of Complex Variables. New York: Schaum's Outline Series, McGraw-Hill Book Company, 1964.
8. Kuethe, Arnold M. and Chuen-Yen Chow. Foundations of Aerodynamics: Bases of Aerodynamic Design (Third Edition). New York: John Wiley and Sons, Inc., 1976.
9. Milne-Thomson, L.M. Theoretical Aerodynamics (Third Edition). London: MacMillan and Company Limited, 1958.
10. Karamcheti, Krishnamurty. Principles of Ideal-Fluid Aerodynamics. New York: John Wiley and Sons, Inc., 1966.
11. Von Wagner, H. "Dynamischer Auftrieb von Tragflugeln," Zeitschrift fuer Angewandte Mathematik und Mechanik, 5: 17 (February 1925).
12. Giesing, Joseph P. "Nonlinear Two-Dimensional Unsteady Potential Flow with Lift," Journal of Aircraft, 5:135 (March-April 1968).

13. Chow, Chuen-Yen and Ming-Ke Huang. "The Initial Lift and Drag of an Impulsively Started Airfoil of Finite Thickness," Journal of Fluid Mechanics, 118:393-409 (May 1982).



## VITA

Captain Kenneth W. Tupper was born on 22 April 1952 in Johnson City, New York. He graduated from high school in Meadville, Pennsylvania, in 1970 and attended the United States Air Force Academy from which he received the degree of Bachelor of Science in Astronautical Engineering in June 1974. Upon graduation, he was commissioned a Second Lieutenant in the USAF. He completed pilot training and received his wings in July 1975. He served as a KC-135 pilot and flight instructor in the 924th Aerial Refueling Squadron, Castle AFB, California, until entering the School of Engineering, Air Force Institute of Technology, in June 1982.

Permanent address: 978 Northwood Drive  
Merced, California 95340

UNCLASSIFIED

SECURITY CLASSIFICATION OF THIS PAGE

AD-A136 921

## REPORT DOCUMENTATION PAGE

|   |  |   |                      |
|---|--|---|----------------------|
| 1a. REPORT SECURITY CLASSIFICATION<br>UNCLASSIFIED  |  | 1b. RESTRICTIVE MARKINGS  |                      |
| 2a. SECURITY CLASSIFICATION AUTHORITY   |  | 3. DISTRIBUTION/AVAILABILITY OF REPORT<br>Approved for public release;<br>distribution unlimited. |                      |
| 2b. DECLASSIFICATION/DOWNGRADING SCHEDULE   |  |   |                      |
| 4. PERFORMING ORGANIZATION REPORT NUMBER(S)<br>AFIT/GAE/AA/83D-24   |  | 5. MONITORING ORGANIZATION REPORT NUMBER(S)   |                      |
| 6a. NAME OF PERFORMING ORGANIZATION<br>School of Engineering  | 6b. OFFICE SYMBOL<br>(If applicable)<br>AFIT/EN              | 7a. NAME OF MONITORING ORGANIZATION   |                      |
| 6c. ADDRESS (City, State and ZIP Code)<br>Air Force Institute of Technology<br>Wright-Patterson AFB, Ohio 45433   |  | 7b. ADDRESS (City, State and ZIP Code)  |                      |
| 8a. NAME OF FUNDING/SPONSORING ORGANIZATION   | 8b. OFFICE SYMBOL<br>(If applicable)                         | 9. PROCUREMENT INSTRUMENT IDENTIFICATION NUMBER   |                      |
| 8c. ADDRESS (City, State and ZIP Code)  |  | 10. SOURCE OF FUNDING NOS.  |                      |
|   |  | PROGRAM ELEMENT NO.   | PROJECT NO.          |
|   |  | TASK NO.  | WORK UNIT NO.        |
| 11. TITLE (Include Security Classification)<br>See Box 19   |  |   |                      |
| 12. PERSONAL AUTHOR(S)<br>Kenneth W. Tupper, B.S., Capt, USAF   |  |   |                      |
| 13a. TYPE OF REPORT<br>MS Thesis  | 13b. TIME COVERED<br>FROM _____ TO _____                     | 14. DATE OF REPORT (Yr., Mo., Day)<br>1983 December   | 15. PAGE COUNT<br>80 |
| 16. SUPPLEMENTARY NOTATION<br>Approved for public release: IAW AFR 190-17.<br><i>John Wolan</i><br>LYN E. WOLANER<br>Dean for Research and Professional Development<br>Air Force Institute of Technology (AFIT) |  |   |                      |
| 17. COSATI CODES  |  | 18. SUBJECT TERMS (Continue on reverse if necessary and identify by block number)                 |                      |
| FIELD   | GROUP  | SUB. GR.  |                      |
| 20  | 04   | Wake Vortex Effects, Dynamic Stall, Potential Flow Vortex Wake, Starting Vortex                   |                      |
| 19. ABSTRACT (Continue on reverse if necessary and identify by block number)  |  |   |                      |
| Title: THE EFFECT OF TRAILING VORTICES ON THE PRODUCTION OF LIFT ON AN AIRFOIL UNDERGOING A CONSTANT RATE OF CHANGE OF ANGLE OF ATTACK  |  |   |                      |
| Thesis Advisor: Eric J. Jumper, Major, USAF   |  |   |                      |
| 20. DISTRIBUTION/AVAILABILITY OF ABSTRACT<br>UNCLASSIFIED/UNLIMITED <input checked="" type="checkbox"/> SAME AS RPT. <input type="checkbox"/> DTIC USERS <input type="checkbox"/>                               |  | 21. ABSTRACT SECURITY CLASSIFICATION<br>UNCLASSIFIED  |                      |
| 22a. NAME OF RESPONSIBLE INDIVIDUAL<br>Eric J. Jumper, Major, USAF  | 22b. TELEPHONE NUMBER<br>(Include Area Code)<br>513-255-2998 | 22c. OFFICE SYMBOL<br>AFIT/EN   |                      |

DD FORM 1473, 83 APR

EDITION OF 1 JAN 73 IS OBSOLETE.

UNCLASSIFIED  
SECURITY CLASSIFICATION OF THIS PAGE

This study explored the effect of a trailing vortex wake on the production of lift on an airfoil undergoing a constant rate of change of angle of attack,  $\dot{\alpha}$ . The study showed that when an airfoil encounters a constant- $\dot{\alpha}$  flow, the trailing vortex wake acts to suppress the slope of the airfoil's  $C_l$  vs.  $\alpha$  curve. The change in magnitude of this effect as a function of airfoil thickness and camber was also investigated.

Potential flow theory was used to model the flow about a two-dimensional circular cylinder, and that flow was transformed to flow about an airfoil by the Joukowski transformation. The trailing vortex wake was modeled by a sequence of discrete point vortices, and the pitching motion of the airfoil was modeled by a series of small incremental changes in angle of attack,  $\Delta\alpha$ , over a short period of time,  $\Delta t$ . The rate of change of angle of attack,  $\dot{\alpha}$ , was then defined as  $\Delta\alpha/\Delta t$ . After each time change  $\Delta t$ ,  $\alpha$  was changed by an amount  $\Delta\alpha$ . A discrete vortex was introduced into the wake at a distance  $U_\infty\Delta t$  behind the airfoil trailing edge, and a bound vortex of equal strength but opposite sense was introduced to satisfy the Kutta condition and keep the total circulation in the flow field equal to zero. As each new vortex pair was introduced, all other trailing vortices were assumed to move in the wake by a distance  $U\Delta t$ , where  $U$  is the velocity induced at a vortex position by all other trailing vortices, the bound vortices, and the free stream flow. The unsteady Bernoulli equation was solved using numerical integration and differentiation techniques to determine pressure difference distribution, vorticity distribution, and coefficient of lift on the airfoil for that instant in time. This information was then used to investigate the overall effect of constant- $\dot{\alpha}$  flow as well as the effect of thickness and camber on the constant- $\alpha$  problem, and simple rules for predicting the effects were developed.